Water Resources Research

RESEARCH ARTICLE
10.1029/2022WR034155

Special Section:
The Future of Critical Zone Science: Towards Shared Goals, Tools, Approaches and Philosophy

Upland Hillslope Groundwater Subsidy Affects Low-Flow Storage–Discharge Relationship

Hongyi Li[1] and Ali A. Ameli[1]

[1]Department of Earth, Ocean and Atmospheric Sciences, The University of British Columbia, Vancouver, BC, Canada

Key Points:

- Upland hillslope groundwater subsidy increases the nonlinearity of low-flow dynamics and alters the shape of storage–discharge relation
- Hydraulic groundwater theory explains the estimated low-flow nonlinearity in a portion (but not all) of the study catchments
- Catchments with a limited extent of upland hillslope groundwater subsidy may be more low-flow vulnerable than catchments with a larger upland subsidy

Supporting Information:

Supporting Information may be found in the online version of this article.

Correspondence to:

A. A. Ameli,
aameli@eoas.ubc.ca

Citation:

Li, H., & Ameli, A. A. (2023). Upland hillslope groundwater subsidy affects low-flow storage–discharge relationship. *Water Resources Research*, *59*, e2022WR034155. https://doi.org/10.1029/2022WR034155

Received 20 NOV 2022
Accepted 7 SEP 2023

Author Contributions:

Conceptualization: Ali A. Ameli
Data curation: Hongyi Li
Formal analysis: Hongyi Li
Funding acquisition: Ali A. Ameli
Methodology: Hongyi Li
Project Administration: Ali A. Ameli

Abstract Large-scale cross-site scientific synthesis on low-flow storage–discharge relation can promote developing transferable hypotheses on the interactions among critical zone attributes and on how such interactions affect catchments' water vulnerabilities. This study leverages cross-site empirical and theoretical analyses and develops a similarity index, based on the interactions among critical zone attributes, to help determine the less-explored influence of upland hillslope groundwater subsidy on storage–discharge relation. We show that an increase in the relative extent of upland hillslope groundwater subsidy to low-flow discharge, occurring through deep slow low-moving (e.g., bedrock) storage unit, leads to (a) an increase in the nonlinearity of low-flow discharge sensitivity to storage (β_1) and (b) an increase in the convexity of low-flow storage–discharge relation. Our findings also raise new hypotheses on the applicability of Boussinesq-based hydraulic groundwater theory at low-flow condition. Empirical results show that in a portion of our study catchments, particularly in those with a relatively small extent of upland hillslope groundwater subsidy, the theory's proposed range of nonlinearity sufficiently explains the nonlinearity of low-flow storage–discharge relation. However, in catchments with a strong influence of upland hillslope groundwater subsidy through deep slow-moving storage unit, the current state of hydraulic groundwater theory, using one single (non)linear representative storage unit, may not be sufficient to explain the large nonlinearity and convexity of low-flow storage–discharge relation (or the long tail of hydrograph late recession). Considering β_1 informs the low-flow vulnerability of catchments, the findings of this study deepen and generalize our understanding of where low-flow discharge is vulnerable to storage's change.

Plain Language Summary There is limited knowledge of the ways watersheds generate stream low flow during dry periods, in watersheds with no (or little) streamflow observations and even in watersheds with extensive streamflow observations. This knowledge gap can limit the development of accurate models and hinder assessments of the impacts of global environmental changes on drought vulnerability. This study aims to address this knowledge gap by examining the a less-explored way in which watersheds may generate a large amount of streamflow during dry periods from upland hillslopes located tens to hundreds of kilometers away from the mainstream. Our study shows that in some environments, this poorly quantified component of water balance may disproportionately (a) affect the relationship between watershed storage and streamflow discharge, which is used to develop a hydrologic model, and (b) contribute to the long tail of streamflow hydrograph during dry periods and thus reducing the vulnerability of drought. Our findings suggest that while the classical theory of streamflow generation can sufficiently explain the ways watersheds generate stream low flow in a portion of watersheds, the large contribution from upland hillslopes to low flow may result in certain watersheds being less low-flow vulnerable than others.

1. Introduction

Critical zone science has made significant advancements in bringing together various disciplines. Yet, the poorly studied interactions and coevolution among soil, rock, topography, land cover, and climate hinder us from developing a quantitative and generalizable understanding of hydrologic storage–discharge relation in the critical zone (L. Li et al., 2017; Sivapalan, 2018). This challenge is especially true at stream low flow, where a potentially large discharge from hillslopes bedrock storage remains poorly characterized and quantified (Hale et al., 2016). Nevertheless, large-scale scientific synthesis on how catchments store and discharge water at a low-flow state can stimulate (transferable) understanding of the interactions between water, rock, and energy in the critical zone and their connections to the low-flow storage–discharge relation (Wlostowski et al., 2021). Such insight could shed light on (a) the regionalization of storage–discharge relation to ungauged landscapes (Blöschl et al., 2014; Hrachowitz et al., 2013), (b) the catchment's drought vulnerability to the rapidly changing environment (Ameli

Software: Hongyi Li
Supervision: Ali A. Ameli
Validation: Hongyi Li, Ali A. Ameli
Visualization: Hongyi Li
Writing – original draft: Ali A. Ameli
Writing – review & editing: Hongyi Li

& Creed, 2018; Brooks et al., 2015), and (c) the patterns of stream transit time and that of concentration of geogenic and biogenic solutes in natural and agricultural landscapes (Ameli et al., 2017; L. Li et al., 2022). A qualitative synthesis of the linkages between the critical zone structure, stream low-flow generation mechanisms, and low-flow discharge sensitivity to changes in storage has been recently conducted by Wlostowski et al. (2021) across 15 (mostly) small catchments in the USA-Critical Zone Observatories (CZOs). Inspired by this qualitative synthesis, the present study aims to contribute to developing a more generalizable quantitative framework to interrogate the linkages between critical zone structure and low-flow storage–discharge relation across a suite of climatic and physical settings.

The streamflow sensitivity to changes in subsurface storage, also referred to as the *sensitivity function*, was introduced by Kirchner (2009) as a product of the classical recession analysis (Brutsaert & Nieber, 1977). The sensitivity function can be used to characterize catchment-scale flow dynamics and estimate the functional form of the storage–discharge relationship. The sensitivity function has been widely used to identify the nonlinear relation between subsurface dynamic storage and discharge (Birkel et al., 2011), describe the average flow and low-flow vulnerabilities to alterations in subsurface storage (Berghuijs et al., 2016; Teuling et al., 2010), explore functional relationships between rainfall variability and catchment transit time (Wilusz et al., 2017), calculate groundwater recharge to high-elevation bedrock systems (Ajami et al., 2011), estimate catchment dynamic storage (Buttle, 2016; Carrer et al., 2019), and assess catchment dynamic storage variations over time due to permafrost thawing (Cooper et al., 2023). Tashie et al. (2020) suggested that the nonlinearity of the sensitivity function (β: the value of sensitivity function power law exponent) could provide valuable insights into catchments' drought vulnerability. Indeed, a larger β implies a more convex hydrograph recession, indicating a sustained long tail at the late recession with a relatively more stable and drought-resistant low-flow condition. Additionally, a larger β implies a more convex storage–discharge relation, indicating a smaller variation in low-flow discharge for a unit change in subsurface storage. Hereafter, in this paper, a larger nonlinearity corresponds to a larger β and a more significant convexity of storage–discharge relation. Thus, for the case in which the relation is concave ($\beta < 0$), larger nonlinearity still refers to a relatively larger convexity (which is equivalent to a smaller concavity; see Tashie et al., 2020).

The nonlinearity of sensitivity function (β)—proportional to the nonlinearity of storage–discharge relation and that of hydrograph recession (see Section 3.1)—is theoretically explained by two different theories. Hydraulic groundwater theory relates the nonlinearity of hydrograph recession, at both early and late recession stages, to the nonlinear hydraulic of flow during water discharge from a single "representative storage unit" (Brutsaert & Nieber, 1977). This explanation is based on derivations from the Boussinesq equation, which assumes that the catchment-scale storage–discharge relation follows that of a representative storage unit whose hydraulic properties (e.g., water transmission function) are representative of the hydraulic properties of the collection of units (i.e., soil mantled shallow aquifers, bedrock aquifers) that make up a catchment. For late-recession nonlinearity (β_1), which is assumed to represent the nonlinearity of low-flow state, this theory suggests a range of β_1 between -1 and 0.5 for different morphology, geology, and climate conditions of the representative storage unit (see review paper by Troch et al. [2013] and see the discussion in Section 5.2 for more details). Catchment hydraulic properties, however, could be vastly different among storage units in some environments. Thus, a single storage unit may not sufficiently represent catchment flow dynamics. The variability theory (Harman et al., 2009), a more recent theory, links the nonlinearity of "overall" recession (merged early and late recession stages) to the variability of subsurface flow hydraulic among the storage units that make up a catchment. Using a multiple linear reservoir model, Harman et al. (2009) theoretically showed that the nonlinearity of hydrograph recession is strongly associated with the variability of time constants among linear reservoirs. In their theoretical model, a linear reservoir was assumed to emulate the storage–discharge behavior of each storage unit, with the reservoir's time constant reflected the unit's transmission timescale. Furthermore, Clark et al. (2009), using streamflow data at three different scales within Panola experimental catchment, showed that discharges from three storage units with distinct transmission timescales, including hillslopes, ephemeral riparian zone, and permanent riparian zone, sequentially increase the nonlinearity of overall recession.

Progress has been made in developing different theories—and conceptual models—that can explain the nonlinearity of "overall" recession. However, overall recession merges a wide range of recession flow dynamics. The strong nonlinearity of early recession could dominate the overall recession nonlinearity, concealing the information on low-flow storage–discharge relation one can extract from the hydrograph recession (Kim et al., 2023). Therefore, the theories and conceptual models of the overall recession may not be transferrable to late-recession

dynamics. While the studies used the variability theory focused mainly on the overall recession, hydraulic groundwater theory suggested a separate theoretical range for the late-recession nonlinearity (as stated above). However, this theoretical range was not explored empirically across different climatic and physical settings to allow generalization to diverse environments. More importantly, it was not explored whether a single "representative storage unit" could thoroughly explain the combinations of diverse mechanisms which are involved in the catchment's late-recession dynamics. Generally, hydraulic groundwater theory, variability theory, and other conceptual models used to describe hydrograph recession, sensitivity function, and storage–discharge relation were not translated into a generalizable framework able to rationalize and estimate the nonlinearity of hydrograph's late recession or that of low-flow storage–discharge relation (Troch et al., 2013).

Subsurface discharge to low flow can be sourced from different storage units of a given catchment. A riparian sedimentary deposit aquifer is a relatively shallow storage unit that (almost) always contributes relatively fast-moving groundwater to low flow (Klaus et al., 2015). Gabrielli et al. (2018)—through an intensive geochemical and hydrometric field campaign over 400 days at the Maimai catchment in New Zealand—showed that a large proportion of low flow during both wet and dry seasons comes from riparian sedimentary deposit aquifer with less than 4 months old groundwater age. They also showed that there is an additional independent storage unit that contributes distinctly older groundwater to low flow. A deep slow-moving (bedrock) aquifer that connects upland hillslope bedrock groundwater to riparian bedrock and ultimately contributes to stream low flow, with minimal interaction with shallow riparian sedimentary deposit aquifer. Their experimental analysis depicted an average groundwater age of 10.5 years within upland hillslope bedrock and of 23 years old within deep riparian bedrock near the discharge zone. Ameli et al. (2018) modeling experiment in the same site showed that despite having low-permeable bedrock, close to 50% of water recharged in the Maimai upland hillslopes subsidizes their mainstream through deep slow-moving bedrock aquifer.

At Maimai catchment, both shallow fast-moving riparian and deep slow-moving storage units proportionally and independently contribute to low flow. The stream's low-flow transit time reflected the groundwater ages of both storage units, while groundwater ages at the discharge points of the two storage units were distinctly different (4 months vs. 23 years; Gabrielli et al., 2018). At a relatively more permeable Scottish catchment (with surficial geology composed of glacial drift), Birkel et al. (2015) showed that upland hillslope groundwater contribution through deep slow-moving aquifer is the dominant source of low flow as stream low-flow transit time largely reflects the old age of this storage unit. These experimental findings may suggest that upland hillslope groundwater subsidy, occurring through deep slow-moving aquifer, should be incorporated in theories and conceptual models of low-flow generation. Upland groundwater contribution through deep slow-moving aquifer—or *groundwater subsidy* to parent catchment as termed by Ameli et al. (2018)—may have distinctively older age, longer transmission timescale, and different geochemical function compared to groundwater contribution through shallow riparian sedimentary deposit aquifer. As suggested by the two experimental examples above and shown by the modeling experiment conducted by Ameli et al. (2018), the relative extent of groundwater subsidy varies from one catchment to the other, depending on the catchment's climatic, topographical, and geological characteristics.

In this paper, we hypothesize that the extent of upland hillslope groundwater subsidy influences the nonlinearity of sensitivity function or that of storage–discharge relation dominating low flow. A relatively large volume of upland hillslope groundwater subsidy through deep slow-moving aquifer (such as bedrock aquifer) in addition to the consistently accessible groundwater supply from the shallow fast-moving riparian sedimentary deposit aquifer may increase low-flow nonlinearity of sensitivity function. This is caused by the distinct transmission timescales between the two storage units (or aquifers). Alternatively, a relatively small extent of upland hillslope groundwater subsidy through deep slow-moving aquifer makes riparian sedimentary deposit aquifer the primary discharge contributor to low flow, reducing the catchment-scale nonlinearity. In the present study, this hypothesis is tested theoretically and empirically. Our empirical (large-sample hydrology) analysis will be conducted across a large sample of catchments in Canada and the USA. In this analysis, we also develop a Groundwater Subsidy Index (GSI) that approximates the catchment-scale ratio between the groundwater contributions of upland hillslope through deep slow-moving aquifer and riparian shallow sedimentary deposit aquifer. To achieve a process-oriented and generalizable approach, the index includes the hydrologically relevant interactions among landscape critical zone attributes. Our theoretical and empirical analyses also help to evaluate the applicability of the range of nonlinearity values proposed by hydraulic groundwater theory and to generate hypotheses on the potential causes of deviation from the suggested range.

Overall, we respond to Wlostowski et al. (2021) call for the synthesis of low-flow generation mechanisms and build on the conceptual models of overall recession nonlinearity proposed by Harman et al. (2009) and Clark et al. (2009) to develop a generalizable scientific synthesis on how critical zone structure links to a catchment's low-flow sensitivity function and storage–discharge relation. Primarily, we respond to the questions below theoretically and empirically:

Does the extent of upland hillslope groundwater subsidy through deep slow-moving aquifer, relative to the groundwater contribution of shallow riparian sedimentary deposit aquifer, inform developing a generalizable conceptual model able to

1. Describe the nonlinearity of the low-flow sensitivity function?
2. Explain the functional relation between storage and low-flow discharge?

The research questions above are some of the most pressing in understanding critical zone hydrologic processes, as noted in recent reviews (Grant & Dietrich, 2017; Markovich et al., 2019; McDonnell, 2017).

2. Data

2.1. Streamflow Data

The streamflow data contain 1,798 gauges across Canada and the United States. The Canadian gauges are from the HYDAT data set (Water Survey of Canada [2020], HYDAT database), while the United States stream gauges are from the CAMELS data set (Addor et al., 2017). The 1,798 catchments, associated with these gauges, have areas ranging from 100 to 289,128 km^2, where catchments smaller than 100 km^2 were excluded due to the coarse resolution of climatic attributes (as done in Janssen & Ameli, 2021; Wu et al., 2021). The details of catchment boundary polygon delineation and catchment area calculation are explained in Section 2.3. Note that these catchments were minimally impacted by land development practices. Streamflow data from these 1,798 catchments, for the period between 1 January 1981 and 31 December 2019, were used to calculate the streamflow sensitivity function and storage–discharge relation (see Section 3.3). For each catchment, to calculate the proposed GSI (Section 3.4), the catchment-scale average values of climatic, topographical, soil, and geological attributes were calculated using available databases and delineated catchment boundary polygon, as will be explained in Sections 2.2–2.4.

2.2. Climatic Data

Climatic data used in our study were obtained from the ERA5-Land (ERA5-L) database (Muñoz-Sabater et al., 2021) for the period between 1 January 1981 and 31 December 2019. ERA5-L provides estimated monthly averaged global climatic data on land masses at 9 km^2 spatial resolution. In each catchment, we used monthly scale total precipitation, snowmelt, and actual evapotranspiration data to calculate the long-term average annual water surplus and snow fraction, during the study period (1981–2019). The former was calculated as the long-term average of the annual water surplus, where the annual water surplus was calculated as the sum of differences between monthly total precipitation and monthly total actual evapotranspiration in each year. The latter was calculated as the ratio of the long-term average annual snowmelt to the long-term average annual total precipitation. We used one single globally available database of climatic attributes to showcase the potential application of the proposed index in our empirical analysis to the other parts of the globe. In addition, the use of one single database for all interrelated climatic data helps reduce the systematic bias in estimating our index and ultimately in testing our hypothesis. In our case, most available local and regional climatic databases in North America, which contain precipitation and snowmelt data, do not include actual evapotranspiration.

2.3. Topographical Data

For each Canadian catchment, we used 90-m^2 resolution elevation, flow direction, and flow accumulation raster-based data from MERIT Hydro (Yamazaki et al., 2019) to delineate the catchment boundary polygon using the Watershed Tool in ArcGIS. The USA's catchments boundary polygons were delineated in a similar manner in Addor et al. (2017). The delineated boundary polygons were used to calculate catchment-scale average values of climatic (Section 2.2) and soil and geological attributes (Section 2.4). The elevation data were also used to

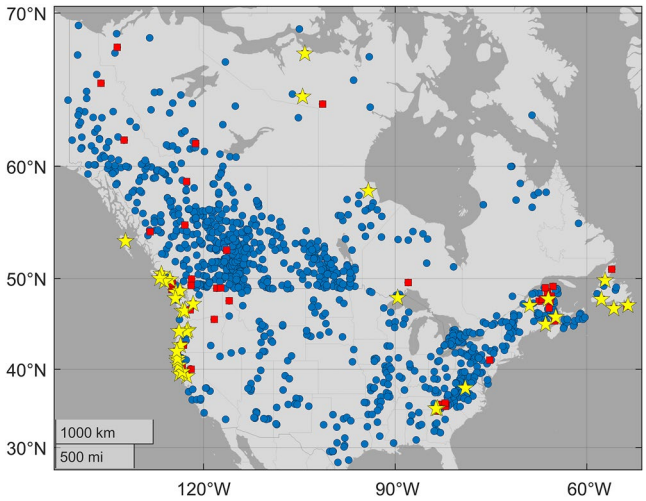

Figure 1. The locations of 1,137 study catchments. A total of 78 red squares and yellow stars refer to the catchments used in the Base Case methodological scenario after applying the associated filters (see Section 3.3). Yellow stars refer to the 37 catchments that remained in the Bootstrap methodological scenario after bootstrapping the data and applying the associated filters (see Text S2 in Supporting Information S1).

calculate the raster-based slope at 90-m resolution. Then, using the delineated boundary polygons, we calculated the catchment-scale average value of slope for each study catchment.

2.4. Soil and Geological Data

The soil hydraulic conductivity data were extracted from a gridded (900-m^2 resolution) global-scale database developed by Dai et al. (2019) to calculate catchment-scale average soil hydraulic conductivity (K_{soil}) and catchment-scale standard deviation of soil hydraulic conductivity. The average (K_d) and standard deviation of saturated hydraulic conductivity of deep geological formation were calculated for each catchment using global-scale data set on the permeability of deep geology developed by Huscroft et al. (2018). The catchment-scale average sedimentary deposit thickness (SDT) and catchment-scale standard deviation of SDT were estimated using 1-km^2 resolution SDT data compiled by Pelletier et al. (2016). Here, we calculated the catchment-scale standard deviation of soil and geological properties additional to their catchment-scale average. We assume that in those catchments with a large within-catchment variability (or standard deviation) of these attributes, the average values of the attributes cannot be meaningful representatives of catchments shallow and deep hydraulic characteristics. Therefore, 661 out of the 1,798 catchments with standard deviations of K_{soil}, K_d, or SDT larger than 30% are excluded from our study catchments. This left us with 1,137 catchments (Figure 1) for further analysis. It should be noted that the use of other magnitudes for this filter (e.g., 40%) does not affect the conclusions of this study. Additionally, we used the 1-km^2 resolution raster-based global-scale data set on the percentage of hillslope versus riparian zone, developed by Pelletier et al. (2016). We calculated the catchment-scale average percentage of hillslope versus riparian zone for each study catchment.

3. Method

In this section, we present the methodology and analytical framework employed in our study. First, we introduce the equations of sensitivity function, storage–discharge relation, and the description of their nonlinearities (Section 3.1). Next, using two linear reservoir model, we derive an analytical equation for the nonlinearity of sensitivity function at low flow (β_1) as a function of hydraulic properties of the two reservoirs contributing groundwater to low flow (Section 3.2). The first reservoir emulates shallow fast-moving riparian sedimentary deposit aquifer and the second reservoir emulates deep slow-moving aquifer. This analysis helps us to theoretically explore our overarching hypothesis (as we will be explained in Section 4). Sections 3.3–3.5 explain the methodologies used in our empirical analyses. Section 3.3 explains our methods used to derive β_1 using streamflow observation data. Then, we develop a GSI, composed of hydrologically relevant interactions among critical zone attributes, to approximate the ratio of upland hillslope groundwater subsidy through deep slow-moving aquifer to groundwater contribution through shallow fast-moving riparian sedimentary deposit aquifer (Section 3.4). Finally, we explore the general association between the GSI and β_1 (and the nonlinearity of storage–discharge relation) across a large sample of catchments spanning a spectrum of climatic, topographical, and geological conditions (as explained in Section 3.5).

3.1. Sensitivity Function and Storage–Discharge Relation

The hydrograph recession analysis, proposed by Brutsaert and Nieber (1977), has been widely used to study catchment-scale flow dynamics. The relation between recession rate ($-dQ/dt$) and streamflow (Q), in the log–log scale, is often approximated as linear suggesting a power law relationship between recession rate and streamflow as

$$-\frac{dQ}{dt} = aQ^b \quad (1)$$

where a and b are recession constants. The exponent b is recently called the hydrograph recession nonlinearity (Tashie et al., 2020). Kirchner (2009) derived the sensitivity function ($g(Q)$) [1/T] or streamflow sensitivity to changes in subsurface storage as

$$g(Q) = \frac{dQ}{dS} = \frac{dQ/dt}{dS/dt} \tag{2a}$$

$$g(Q) \approx -\frac{dQ/dt}{Q} = aQ^{\beta} \tag{2b}$$

The power function's exponent (β) refers to the nonlinearity of the sensitivity function. Note that Equation 2b was approximated from Equation 2a, assuming minimal human interference in the catchment and during the periods with the minimal surface flow and when ET (actual evapotranspiration) and P (precipitation) are much smaller than Q. $g(Q)$ function can also be used to identify the relationship between storage (S–S_0) and discharge (Q), as done in Carrer et al. (2019):

$$S - S_0 = \begin{cases} \frac{1}{a} \cdot \frac{1}{1-\beta} Q^{1-\beta}, \beta \neq 1 \\ \frac{1}{a} \ln(Q), \beta = 1 \end{cases} \tag{3}$$

Here, S–S_0 refers to the active (or hydraulic) storage, where S_0 in a given catchment is the subsurface storage corresponding to an arbitrary reference Q value (e.g., minimum storage corresponds to a minimum of late-recession flow value extracted along all recession events; see Figures 2c and 2d for the examples of storage–discharge relations calculated using Equation 3).

The term "nonlinearity" will be used interchangeably to refer to the nonlinearities of hydrograph recession, sensitivity function, or storage–discharge relation. The power function holds for all three characteristics, where the exponent b, or nonlinearity of hydrograph recession (Equation 1), is related to the exponent β, or nonlinearity of sensitivity function (Equation 2b), by $b = \beta + 1$. The power function's exponent $(1 - \beta)$ refers to the nonlinearity of the storage–discharge relation (Equation 3). Note that a larger recession nonlinearity (or a larger b) refers to a longer tail of hydrograph recession. Similarly, a larger nonlinearity of sensitivity function refers to a larger β and a more significant convexity of storage–discharge relation where storage and discharge represent horizontal axes and vertical axes, respectively. Thus, for the case in which the storage–discharge relation is concave ($\beta < 0$), larger β still refers to a relatively larger convexity (which is equivalent to a smaller concavity) of the storage–discharge relation (see Figure 3 for the conceptual definitions of the nonlinearity and convexity/concavity in hydrograph recession and storage–discharge relation).

3.2. Theoretical Assessment of Our Hypothesis Using Two Linear Reservoir Model

Two (or multi) linear reservoir models (e.g., Gao et al., 2017) could, in a simplified manner, emulate the recession flow dynamics. Clark et al. (2009) conceptual model of recession flow dynamics at the Panola experimental site—built on the multilinear reservoir model of Harman et al. (2009)—suggested that a model with parallel linear reservoirs provides the most plausible explanation for the nonlinearity of overall recession hydrograph. In their conceptualizations, reservoirs with different transmission timescales represented different storage units, including hillslope zone, ephemeral riparian zone, and permanent riparian zone. While the parallel linear reservoir model has often been used to explain the nonlinearity of the overall recession hydrograph, in this study, we use the model to explain the nonlinearity of the sensitivity function that dominates low flow (β_1), conceptually associated only with the late-recession hydrograph. We treated the low flow or late-recession flow ($Q(t)$) in a given catchment as the outcome of the groundwater flow contributions from two parallel linear reservoirs: (a) deep slow-moving aquifer (second reservoir) that emulates hydraulic properties of deep low-permeable strata (e.g., bedrock, lower soil horizons) and connects upland hillslope groundwater subsidy to stream and (b) shallow fast-moving riparian sedimentary deposit aquifer (first reservoir):

$$Q(t) = Q_{\mathrm{d}}(t) + Q_{\mathrm{s}}(t) = Q_{\mathrm{d}}(0)e^{-t/\tau_{\mathrm{d}}} + Q_{\mathrm{s}}(0)e^{-t/\tau_{\mathrm{s}}} \tag{4}$$

$Q_{\mathrm{d}}(t)$ and $Q_{\mathrm{s}}(t)$ refer to the groundwater flow contributions to late-recession flow at time t from deep and shallow aquifers (reservoirs), respectively. τ_{d} and τ_{s} are the time constants of groundwater transmission from deep and

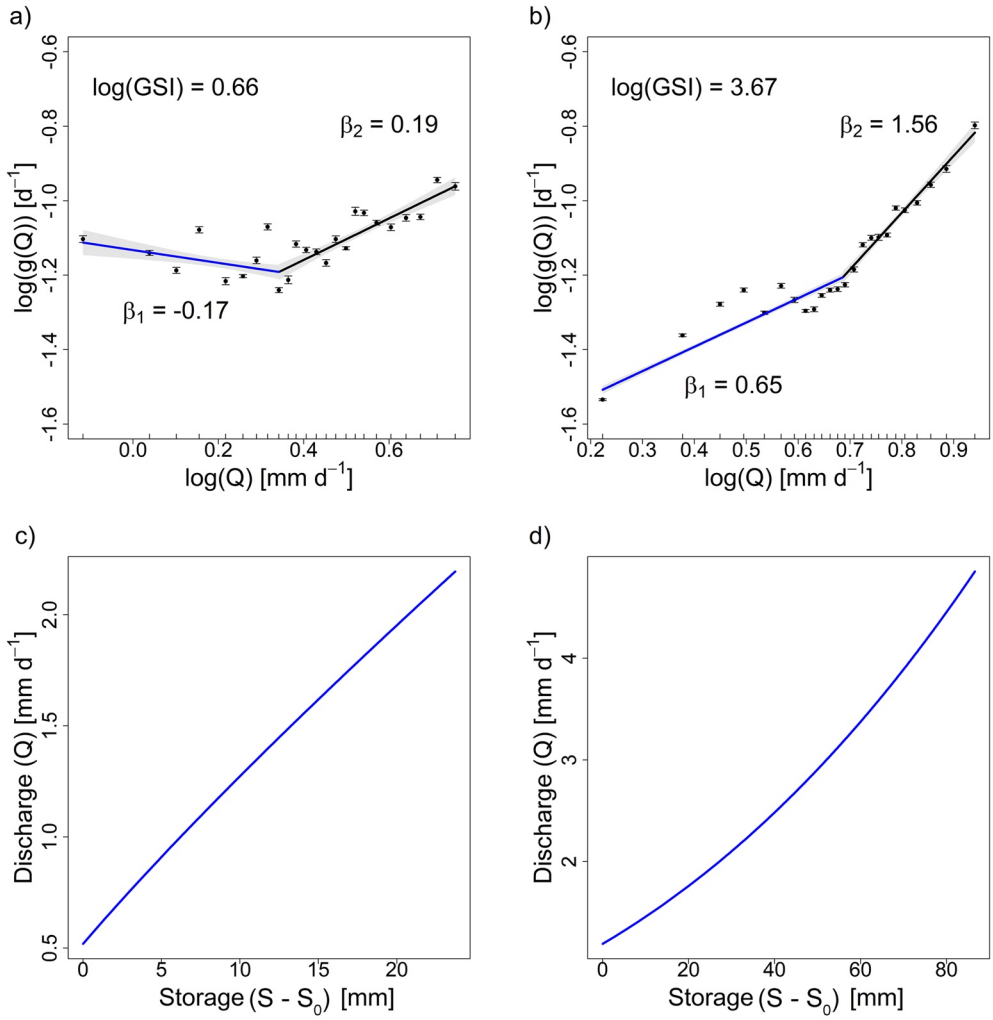

Figure 2. Example estimation of sensitivity function nonlinearity (β) using Base Case methodological scenario for (a) South Toe River Near Celo, North Carolina, USA, and (b) Zeballos River Near Zeballos, British Columbia, Canada. The schematic of storage–discharge relation at low-flow condition corresponding to flow dynamics before the breakpoint (shown in blue in top panels) for (c) South Toe River Near Celo, with a smaller nonlinearity of low-flow sensitivity function (β_1) and a concave low-flow storage–discharge relation, and for (d) Zeballos River, with a larger β_1 and a convex low-flow storage–discharge relation. Here, $S - S_0$ refers to the active (or hydraulic) storage calculated for the late-recession period (before the breakpoint). S_0 is the subsurface storage corresponding to an arbitrary reference Q value (e.g., storage corresponds to a minimum of late-recession flow value extracted along all recession events), in a given catchment.

shallow aquifers. Combing Equations 4 and 2b results in an analytical equation that relates β_1 to Q_d, Q_s, and their time constants (see Text S1 and Equation A8 in Supporting Information S1). The derived equation is comparable to that of Gao et al. (2017), developed for the relationship between the overall recession nonlinearity (b) and compartmentalized flow.

Note that the focus of our paper is to explore the spatial variations of the (time-invariant) "typical" β_1 among catchments and understanding theories and drivers of such spatial variations, rather than assessing the temporal event-to-event variability of β_1 within a single catchment. Therefore, hereafter we assume that two linear reservoir model emulates the typical and the most frequent (among all events) low-flow recession dynamics of a given catchment, and β_1 emulates the typical nonlinearity of low-flow dynamics. This treatment is consistent with the classical application of the (non)linear reservoir model used to explain the typical nonlinearity of storage–discharge relation dominating low flow (e.g., Wittenberg, 1999 among others). In the remainder of this section, we describe how we expand Equation A8 in Supporting Information S1 to obtain a relationship between β_1 and hydraulic properties that control reservoirs flow and their time constants.

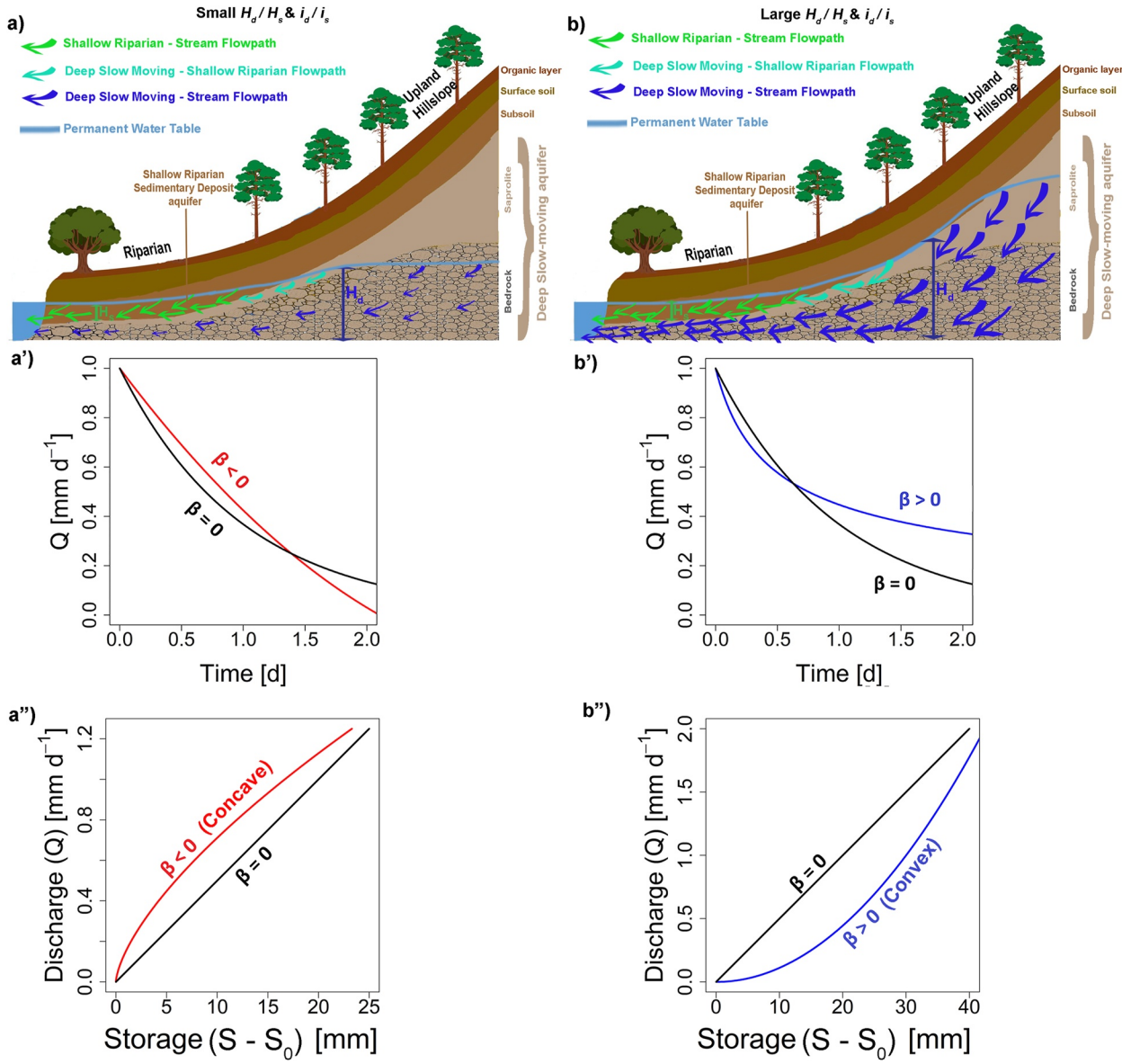

Figure 3. Conceptualization of the overarching hypothesis of this paper. In this conceptualization, the representative shallow fast-moving riparian sedimentary deposit aquifer (depicted by light brown color) represents the hydraulic properties of the collection of a catchment's riparian aquifers containing lowland permeable sedimentary deposits above the bedrock. Groundwater contribution to low flow through this aquifer was shown by green arrows. H_s refers to time-invariant typical saturated thicknesses of the representative shallow riparian aquifer. The representative deep slow-moving aquifer (depicted by khaki and tiled khaki colors) represents the hydraulic properties of the collection of aquifers that connect deep groundwater flow paths (dark blue arrows) from upland hillslope to mainstream at low-flow conditions. H_d refers to time-invariant typical saturated thicknesses of the representative deep slow-moving aquifer. i_d and i_s refer to typical hydraulic gradient of the representative deep slow-moving and shallow fast-moving aquifers, respectively. Arrows density schematizes the relative groundwater contributions of deep slow-moving aquifer (dark blue) versus shallow fast-moving riparian sedimentary deposit aquifer (green). (a) A catchment, with a relatively thin typical saturated thickness and/or with a small typical hydraulic gradient in its deep slow-moving aquifer, sustains small amount of diffusive contribution of upland hillslope groundwater to low flow. (a′) This type of catchments may show a small nonlinearity of low-flow sensitivity function (e.g., $\beta_1 < 0$) with a fast-receding hydrograph at late recession (red line) and (a″) a concave low-flow storage–discharge relation (red line). (b) A catchment, with a relatively thick typical saturated thickness and/or with a large typical hydraulic gradient in its deep slow-moving aquifer (excessive convergence of hydraulic head from hillslope toward stream reflects a large gradient), sustains a large amount of diffusive contribution of upland hillslope groundwater to low flow. (b′) This type of catchments may show a large nonlinearity of low-flow sensitivity function (e.g., $\beta_1 > 0$) with a slow-receding hydrograph (blue line) and (b″) a convex low-flow storage–discharge relation (blue line). Our conceptualization implies that upland groundwater through deep slow-moving aquifer could bypass and/or feed the shallow riparian aquifer that contains low-land permeable sedimentary deposits above the bedrock. Our theoretical analysis (Section 3.2), however, neglects the groundwater interaction between deep slow-moving aquifer and shallow riparian sedimentary deposit aquifer (light blue arrows; see the discussion in Section 5.5). Note that these two schematizations consider identical catchment attributes (e.g., slope, geology) for the sake of simplicity of comparison. In reality, differences in groundwater hydraulics shown in this figure (H_s vs. H_d and i_s vs. i_d) depend on differences in catchment attributes (see Section 3.4).

Building on classical Dupuit approximation, in each catchment, Q_d/Q can be calculated as $(T_d.i_d)/(T_d.i_d + T_s.i_s)$ and Q_s/Q as $(T_s.i_s)/(T_d.i_d + T_s.i_s)$. T_d (and i_d) and T_s (and i_s) refer to time-invariant transmissivity (and hydraulic gradient) of the catchment's representative deep slow-moving aquifer and representative shallow riparian fast-moving aquifer, respectively. Thomas et al. (2013) related the time constants of the linear reservoir explaining a catchment low-flow condition to the reservoir's transmissivity (T), porosity (θ), drainage length (D), and the fractural reservoir area contributing to low flow (α), such that τ depends on $\alpha \times \theta/T \times D$. Building on this, we assume that τ_s/τ_d is linearly dependent on $T_d D_d \alpha_s \theta_s / T_s D_s \alpha_d \theta_d$, where s and d subscripts refer to the properties of shallow fast-moving riparian sedimentary deposit aquifer and deep slow-moving aquifer, respectively. We also assume that at the low-flow condition, the variability of drainage length between the two aquifers is negligible, compared to T (and α,θ) variations between the two aquifers, which implies that τ_s/τ_d is linearly dependent on $T_d\alpha_s\theta_s/T_s\alpha_d\theta_d$. With replacing Q_d/Q, Q_s/Q, and τ_s/τ_d by their associated terms in Equation A8 in Supporting Information S1, we obtain

$$\beta_1 = \frac{\frac{T_d}{T_s} \cdot \frac{i_d}{i_s}\left(\frac{\alpha_s}{\alpha_d} \cdot \frac{\theta_s}{\theta_d} \cdot \frac{T_d}{T_s} - 1\right)^2}{\left(\frac{\alpha_s}{\alpha_d} \cdot \frac{\theta_s}{\theta_d} \cdot \frac{i_d}{i_s}\left(\frac{T_d}{T_s}\right)^2 + 1\right)^2} \tag{5}$$

See Figure 3 for further details and conceptualization of the two linear reservoir model developed in this paper. Note that the parallel (or independent) nature of the two reservoirs considered here neglects the potential interactions between the two aquifers (light blue arrows in Figure 3 reflect such an interaction). Furthermore, Equation 5 is valid under the assumptions and approximation stated above. These limitations will be further discussed in Section 5.5.

3.3. Empirical Analysis: Estimation of Sensitivity Function and Storage–Discharge Relation

In this study, the sensitivity function ($g(Q)$) and its nonlinearity in a given catchment, at both early and late recession stages, were estimated by performing a piecewise-weighted linear regression algorithm (Figure 2). The algorithm uses the ensemble characteristics of many recession events (point-cloud), binning the entire data, and fits a piecewise function to different segments of the binned data (as suggested in Kirchner, 2009). This approach focuses on the time-invariant (or central tendency of) flow dynamics at early and/or late recession stages to delineate a "typical" nonlinearity value for a given catchment rather than delineating one nonlinearity value for each event (see Kim et al., 2023 for differences and similarities between the two approaches of the nonlinearity delineation). Here, in combination with piecewise-weighted linear regression, we used six different widely used methods for extracting recession events, estimating recession rate ($-dQ/dt$), and fitting a piecewise function to different segments of sensitivity function. This was done to investigate whether our conclusions are robust against different derivation techniques of sensitivity function nonlinearity. In the next subsection, we introduce our Base Case methodological scenario. Five other variants of the estimation of sensitivity function and its nonlinearity are explained in Text S2 in Supporting Information S1.

3.3.1. Base Case Methodological Scenario

3.3.1.1. Recession Event Extraction

In our base case scenario (denoted as "Base Case" in the remainder of this paper), we extracted the streamflow recession data from 1,137 study catchments from 1981 to 2019. For each catchment, we first computed the recession rate ($-dQ/dt$) or the time derivative of streamflow (Q), using constant time step, and added the constraint that both $-dQ/dt$ and Q must monotonically decrease for at least five consecutive days. The periods satisfying this condition were identified as the "recession events." We also removed the first 3 days of each recession event from our analysis. These two constraints minimize the chance of the selection of recession events in which the contribution of surface flow and precipitation (P) is considerable. Then, we excluded all catchments with less than 50 acceptable recession events during the study period (1981–2019). Similarly, several other studies used the same criteria to extract recession events (see Tashie et al., 2020 for more information and justification of this methodology).

Additionally, to minimize the impact of ET on the selected recession events, we only considered catchments in which the daily average ET during the growing season (May–September) is smaller than twice the growing

season daily average streamflow (i.e., growing season ET/Q < 2). Note that only a small portion of estimated catchment-wide ET may impact the catchment-scale hydraulic storage at late recession (or low-flow condition). For example, Wlostowski et al. (2021), in delineating the low-flow sensitivity function, assumed that only 25% of estimated catchment-wide ET could impact the hydraulic storage that contributes to low flow. Additionally, recent research showed that ERA5-L-assimilated data employed in our study generally overestimate the actual ET across North America (Lu et al., 2021; Martens et al., 2020). Therefore, we expect that the actual ET impacting late recession is much smaller than the estimated catchment-wide ET using ERA5-L and smaller than streamflow in catchments that passed ET/Q < 2 filters during the growing season. In Section 5, we further discuss the influence of this catchment selection filter on our conclusion and generalization.

3.3.1.2. Estimation of Sensitivity Function Parameters

In order to estimate the sensitivity function parameters, we followed a series of steps. For each catchment that passed the above constraints, the extracted recession events and their pairs of $\log\left(-\frac{dQ/dt}{Q}\right)$ and $\log(Q)$ were used to estimate $g(Q)$ function and its nonlinearity. The quantile of $\log(Q)$ was binned into 25 bins, while the standard error and mean of $\log\left(-\frac{dQ/dt}{Q}\right)$ within each bin were calculated. We removed those bins in which the standard error is larger than half of the mean (in a manner similar to Kirchner, 2009). Then, the piecewise linear regression analysis (using the "segmented" package in R) was used to (a) identify a statistically significant breakpoint, which conceptually refers to the streamflow at which the (nonlinearity of) catchment's sensitivity function alters and (b) fit two linear lines to the binned averages before and after the breakpoint in log–log space of sensitivity function $g(Q)$ and streamflow (Q). Note that for the catchments where one breakpoint is deemed statistically significant, the algorithm sets an arbitrary initial breakpoint and then estimates the actual breakpoint iteratively. In fitting two linear lines to the binned averages before and after the breakpoint, the piecewise linear regression was weighted by the reciprocal of the square of the standard error of $\log\left(-\frac{dQ/dt}{Q}\right)$ in each bin. The uncertainty bounds of each line were also calculated using the estimated standard error (see Kirchner, 2009 for more details).

We denoted the slopes of regression lines on the left and right of the breakpoint as β_1 and β_2, respectively, where β_1 refers to the typical nonlinearity of sensitivity function at low-flow conditions (or at late recession), and β_2 refers to the typical nonlinearity of sensitivity function at early recession. a_1 and a_2 were also identified as the intercepts of two linear lines. Figure 2 shows two examples of β_1 and β_2 estimation using the Base Case approach. We further excluded the catchments that (a) did not display a breakpoint (only one catchment among our study catchments that passed previously mentioned filters), (b) the discharge value of the identified breakpoint is below 20 percentile or above 80 percentile of discharge values of all recession events, or (c) the standard error of the first linear slope (β_1) is larger than 0.1. In the end, 78 catchments, out of the initial 1,137 catchments, remained in the Base Case analysis. Table S1 in Supporting Information S1 reports (a) the number of catchments remained after applying the filters of different methods, and (b) the ranges of estimated nonlinearity of sensitivity function using different methods.

3.3.1.3. Estimation of Storage–Discharge Relation

To estimate the low-flow storage–discharge relation in a given catchment, we used Equation 3 and the estimated parameters of low-flow sensitivity function (a_1 and β_1). Here, the estimated storage ($S - S_0$) in a given catchment refers to the catchment's active (or hydraulic) storage during late-recession flow (i.e., calculated based on discharge values and recession parameters before the breakpoint, see blue line in Figure 2). S_0 conceptually refers to a minimum storage corresponding to the minimum of recession flow values extracted along all recession events of a catchment. Figures 2c and 2d show two examples of the estimation of storage–discharge relations at low flow for two catchments with contrasting β_1 values.

3.4. Empirical Analysis: Developing a New Index

We developed a dimensionless index, the GSI, to compare among the catchments the ratio of upland hillslope groundwater subsidy, through the deep slow-moving aquifer, to groundwater contribution through shallow riparian sedimentary deposit aquifer. To test our overarching hypothesis, the components of GSI should be the critical zone attributes that were known to be relevant to the nonlinearity of sensitivity function (or that of recession hydrograph). H. Li and Ameli (2022) showed that catchment-scale average slope (S [–]), hydraulic conductivities of soil (K_{soil} [L/T]) and deep geological formation (K_d [L/T]), soil thickness (ST [L]), water surplus (WS [L]), and

snow fraction (SF [–]) are among the governing factors of hydrograph recession nonlinearity. In exploring these factors, they used continental-scale observational data and a statistical variable importance method that acknowledges causality and interaction among attributes (i.e., Marginal Contribution Feature Importance). Furthermore, Wlostowski et al. (2021) synthesized the low-flow-related knowledge gained over 15 USA-CZO sites and qualitatively concluded that catchments with high values of sensitivity function (or potentially small β_1) receive most of their precipitation as rain and contain low-permeable clay-rich deep geology. In contrast, sites with low values of sensitivity function (or potentially large β_1) receive the majority of precipitation as snow and have more permeable deep geology. Their qualitative synthesis simply suggested that β_1 is positively associated with SF $\times$ K_d. Hence, K_{soil}, K_d, ST, SF, WS, and S can be the components of an index able to explain the nonlinearity of sensitivity function. Note that in the previous studies focused on identifying the dominant drivers of recession nonlinearity, soil thickness (ST) was used and identified as an important factor. In this study, instead, we used riparian SDT data due to the relevancy of these data to flow contribution through shallow riparian sedimentary deposit aquifer. The references to the source data and the algorithms used to calculate catchment-scale average values of all six attributes were discussed in Sections 2.2–2.4.

GSI, or other indices that explain how a catchment functions hydrologically, should acknowledge the hydrologic interactions among critical zone attributes relevant to the given function (as discussed and showcased in Janssen and Ameli (2021) for storage, partitioning, and discharge functions). Undoubtedly, the nonlinearities of the sensitivity function and storage–discharge relation cannot be sufficiently explained by one critical zone attribute alone or a random composition of the attributes without acknowledging the domain knowledge. Instead, it should be explained by the index that acknowledges the domain knowledge on hydrologic interactions—among critical zone attributes—relevant to the nonlinearity of storage–discharge relation. Furthermore, to explore our hypothesis, a catchment's GSI should reflect the ratio of groundwater contribution through a representative deep slow-moving aquifer to groundwater contribution through a representative shallow riparian sedimentary deposit aquifer (i.e., $T_d \times i_d / T_s \times i_s$ based on Dupuit approximation). In this section, we explain how we use (a) the domain knowledge relevant to storage and discharge hydrologic functioning and (b) the critical zone attributes known to affect the nonlinearity of sensitivity function, in order to estimate $T_d \times i_d / T_s \times i_s$ and ultimately calculate GSI. Additionally, in Text S3 in Supporting Information S1, we used the same critical zone attributes to develop two alternative indices (I_1, I_2) using alternative strategies for combining the attributes, without acknowledging the domain knowledge. In Section 4, we report the efficiency of our original index (GSI) and two alternative indices (I_1, I_2) in explaining β_1.

T_d, in a given catchment, is equal to the product of saturated hydraulic conductivity and typical saturated thickness (H_d in Figure 3) of the representative deep slow-moving aquifer. For the first part of the product, we used catchment-scale average saturated hydraulic conductivity of deep geological formation (K_d) [L/T] (see Section 2.4). Regarding the second part, the lower boundary of deep aquifer (e.g., bedrock aquifer) is not known (Condon et al., 2020) and there is no available metric that approximates the aquifer's average saturated thickness. We utilized domain knowledge to estimate H_d by analyzing how climatic, geological, and topographical attributes interact and impact deep storage. Previous field and modeling literature suggested that H_d (or deep slow-moving aquifer storage) depends on (a) the long-term average magnitude of recharge to groundwater system, (b) snow fraction, and (c) catchment slope (e.g., Ameli et al., 2018; Hopp & McDonnell, 2009; Wlostowski et al., 2021). Recharge magnitude is associated with long-term average water surplus and the hydraulic conductivity contrast at the soil–bedrock (or soil-deep geological formation) interface as suggested by Hopp and McDonnell (2009) and later Ameli et al. (2015). Indeed, for two catchments with identical long-term average water surplus (e.g., two adjacent catchments), the one with a larger hydraulic conductivity contrast (i.e., larger K_{soil}/K_d and all else being equal) may drain a lesser portion of water surplus vertically into deep slow-moving aquifer. Therefore, a large magnitude of recharge into deep aquifer requires both large water surplus and small hydraulic conductivity contrast. This implies that H_d is positively associated with $\left(\frac{WS}{K_{soil}/K_d}\right)$. Hence H_d's association with WS and with K_{soil}/K_d is considered to be nonlinear (through interaction), meaning that H_d's association with WS varies at different levels of K_{soil}/K_d (and H_d's association with K_{soil}/K_d varies at different levels of WS). In addition, Wlostowski et al. (2021) synthesis across USA-CZOs suggested that snow-dominated catchments may have more efficient recharge into upland hillslopes groundwater systems compared to rain-dominated catchments (i.e., H_d is positively associated with SF). Moreover, Ameli et al. (2018) combined extensive hydrometric and tracer observations with a sophisticated physically based model to explore the causal relationship between critical zone attributes and deep aquifer storage. They showed that in catchments with sufficiently large recharge magnitude

(or large WS and small K_{soil}/K_d), the storage of deep slow-moving aquifer increases with catchment slope S (i.e., H_d is positively associated with $\frac{WS.S}{K_{soil}/K_d}$). Based on these scientific evidence, H_d should be positively associated with $\frac{WS.S.SF}{K_{soil}/K_d}$, where the latter could be used to compare the relative magnitude of H_d among catchments. We will further discuss the "comparative" nature of our strategy to develop a new index at the end of this section. Note that H_d's association with each component of the above term is nonlinear (through interaction), meaning that H_d's association with each component varies at different levels of other components.

T_s, in a given catchment, is approximated as the product of catchment-scale average saturated soil hydraulic conductivity (K_{soil} [L/T]) and riparian SDT [L]. In doing so, we approximated the hydraulic conductivity of shallow riparian sedimentary deposit aquifer with the catchment-scale soil hydraulic conductivity as the data on sedimentary deposit saturated hydraulic conductivity were not available. In our comparative framework in delineating GSI, this implies that a catchment with a larger catchment-scale soil conductivity (which includes riparian sedimentary deposits) has a larger riparian sedimentary deposit conductivity compared to a catchment with a smaller catchment-scale soil hydraulic conductivity. Additionally, we assumed that the average saturated thickness in the riparian sedimentary deposit aquifer (H_s in Figure 3) is equal to the riparian SDT on the top of the bedrock.

i_d/i_s, in a given catchment, can also be considered to be positively associated with $\frac{WS.S}{K_{soil}/K_d}$. Indeed, for two catchments with identically large recharge into hillslopes deep groundwater system (i.e., large WS and small K_{soil}/K_d), the one with a steeper slope may show a larger value of i_d/i_s compared to the one with a flatter slope wherein i_d and i_s can be of the same magnitude. Again here i_d/i_s association with each component of the above term is nonlinear (through interaction), meaning that i_d/i_s association with each component varies at different levels of other components.

By replacing the terms which are positively associated with T_d, T_s, and i_d/i_s, the GSI takes the form as

$$GSI = \frac{K_d \times S \times WS \times SF}{K_{soil} \times SDT} \quad (6)$$

Furthermore, the individual components in Equation 6 were normalized before GSI calculation. This implies that all attributes vary between 0 and 1. This treatment ensures that no attribute has excessive weight toward the index value due to their disproportionately large or small values, while the attributes' spatial variability and ultimately GSI's spatial variability remained unchanged.

We have to clarify that the value of GSI in a given catchment cannot reflect the exact ratio of upland hillslope groundwater subsidy to riparian shallow groundwater contribution during low-flow condition. However, GSI is a reasonable proxy to compare, among catchments, their relative sources of low flow. In our comparative approach, a catchment with a larger value of GSI has a larger extent of upland hillslope groundwater subsidy (through deep slow-moving aquifer) relative to shallow groundwater contribution (through riparian sedimentary deposit aquifer), in comparison to a catchment with a lower value of GSI. We hypothesize that the former catchment shows a larger β_1 than the latter (see the conceptualizations in Figure 3). Hence, in the spatial comparative analysis proposed in our paper, GSI can be used to explore the association between the spatial (among catchments) variability in the relative sources of low flow and the spatial (among catchments) variability in β_1.

3.5. Empirical Analysis: Spatial Association Between GSI and β_1

In a spatial between-catchment analysis, we calculated the Spearman correlation between GSI (Section 3.4) and the estimated β_1 (Section 3.3), across the study catchments selected by the Base Case analysis (Section 3.3). This analysis was repeated for two alternative combinations used to develop an index of groundwater subsidy (I_1, I_2; Text S3 in Supporting Information S1) and five alternative methodological scenarios used to estimate β_1 (Text S2 in Supporting Information S1).

4. Results

In this section, we first explain the results of our theoretical analysis conducted using two linear reservoir model (Section 4.1). Then, we explore and compare the estimated values and the spatial pattern of β_1 among different methodological scenarios considered in this paper (Section 4.2). Next, we describe the spatial pattern of the GSI

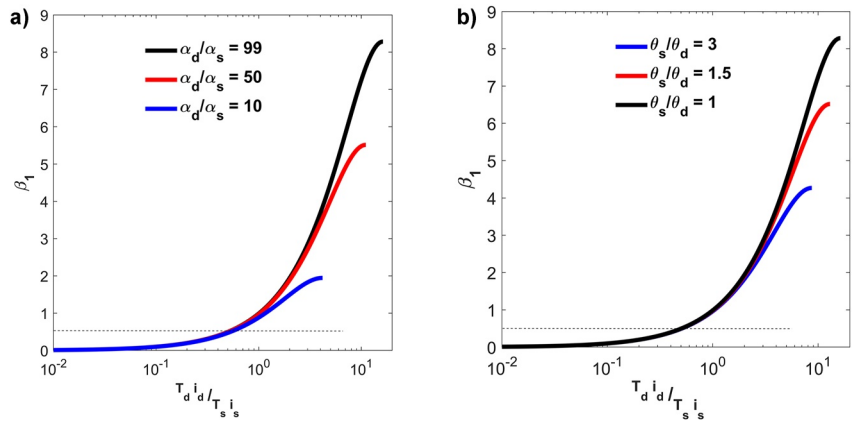

Figure 4. The theoretical relation between the low-flow sensitivity function nonlinearity (β_1) and $T_d \times i_d / T_s \times i_s$ (a) for different levels of α_d/α_s (and $\theta_s = \theta_d$) and (b) for different levels of θ_s/θ_d (and $\alpha_d/\alpha_s = 99$). These plots were generated based on Equation 5 derived using the two linear reservoir model. In this theoretical conceptualization, low flow or late-recession flow in a given catchment is treated as the outcome of the groundwater flow contributions from two parallel linear reservoirs: (1) catchment's representative deep slow-moving aquifer that emulates hydraulic properties of deep low-permeable strata (e.g., bedrock, lower soil horizons) and connects upland hillslope groundwater subsidy to stream, and (2) catchment's representative shallow fast-moving riparian sedimentary deposit aquifer. T_d (and i_d) and T_s (and i_s) refer to typical transmissivity (and hydraulic gradient) of the catchment's representative deep slow-moving aquifer and the representative shallow riparian fast-moving aquifer, respectively. Note that T_d is equal to $K_d \times H_d$, where K_d refers to the average saturated hydraulic conductivity of deep geological formation and H_d (shown in Figure 3) refers to average typical saturated thicknesses of the representative deep slow-moving aquifer. T_s is equal to $K_s \times H_s$, where K_s refers to the saturated hydraulic conductivity of low-land sedimentary deposits above the bedrock in the vicinity of the stream (here is assumed to be equal to K_{soil}, see Section 3.4) and H_s (shown in Figure 3) refers to typical saturated thicknesses of the representative shallow riparian aquifer. α_d and α_s refer to the fractural area of the deep slow-moving aquifer and shallow riparian fast-moving aquifer contributing groundwater to low flow. α_d/α_s for each catchment can be roughly estimated using the catchment-scale average proportion of hillslope versus riparian zone (as explained in Section 2.4). $\alpha_d/\alpha_s = 99$ represents the median value of α_d/α_s across all study catchments in our paper. This ratio was used in this figure to generate some of the potential scenarios on the relation between β_1 and $T_d \times i_d/T_s \times i_s$. In reality, this ratio might be much smaller than 99 in many catchments, as the entire hillslope area of a catchment may not contribute groundwater flow to late-recession flow through deep slow-moving aquifer. θ_d and θ_s refer to the catchment-scale porosity of the representative deep slow-moving and shallow fast-moving aquifers. Dashed line shows $\beta_1 = 0.5$.

as well as the spatial patterns of GSI's components across the study catchments (Section 4.3). Finally, we explore how GSI is associated with the nonlinearity of the sensitivity function (and the functional relation between storage and discharge) in Section 4.4.

4.1. Theoretical Analysis: Two Parallel Linear Reservoir Model

The two linear reservoir model suggests that β_1 depends on $T_d \times i_d/T_s \times i_s$, α_d/α_s, and θ_s/θ_d (Figure 4 and Equation 5). Indeed, β_1 generally increases with $T_d \times i_d/T_s \times i_s$ by a threshold-like relationship. Where $T_d \times i_d/T_s \times i_s < 0.5$, β_1 remains small, and α_d/α_s and θ_s/θ_d have minimal influence on β_1. This implies that for a catchment with a relatively thin saturated thickness and/or with a small hydraulic gradient in its representative deep slow-moving aquifer (e.g., the catchment shown in Figure 3a), β_1 is small and the fractional area of hillslopes contributing groundwater subsidy through deep slow-moving aquifer may have minimal impact on β_1. Where $T_d \times i_d/T_s \times i_s > 0.5$, β_1 significantly increases with an increase in $T_d \times i_d/T_s \times i_s$, particularly for large values of α_d/α_s or θ_d/θ_s. This suggests that for two catchments with a similarly thick typical saturated thickness and similarly large typical hydraulic gradient in their representative deep slow-moving aquifers (e.g., the catchment shown in Figure 3b), the one with a larger fractional area of hillslopes contributing groundwater to low flow and/or with a relatively larger porosity of deep slow-moving aquifer may experience a larger β_1.

4.2. Empirical Analysis: The Estimation of β_1

In this paper, we estimated the nonlinearity of sensitivity function at low flow (β_1) using six different methods, as described in Section 3.3 and Text S2 in Supporting Information S1. The median of estimated β_1 using each method does not differ significantly from one method to the other and varies between 0.08 and 0.37 (Table S1 in

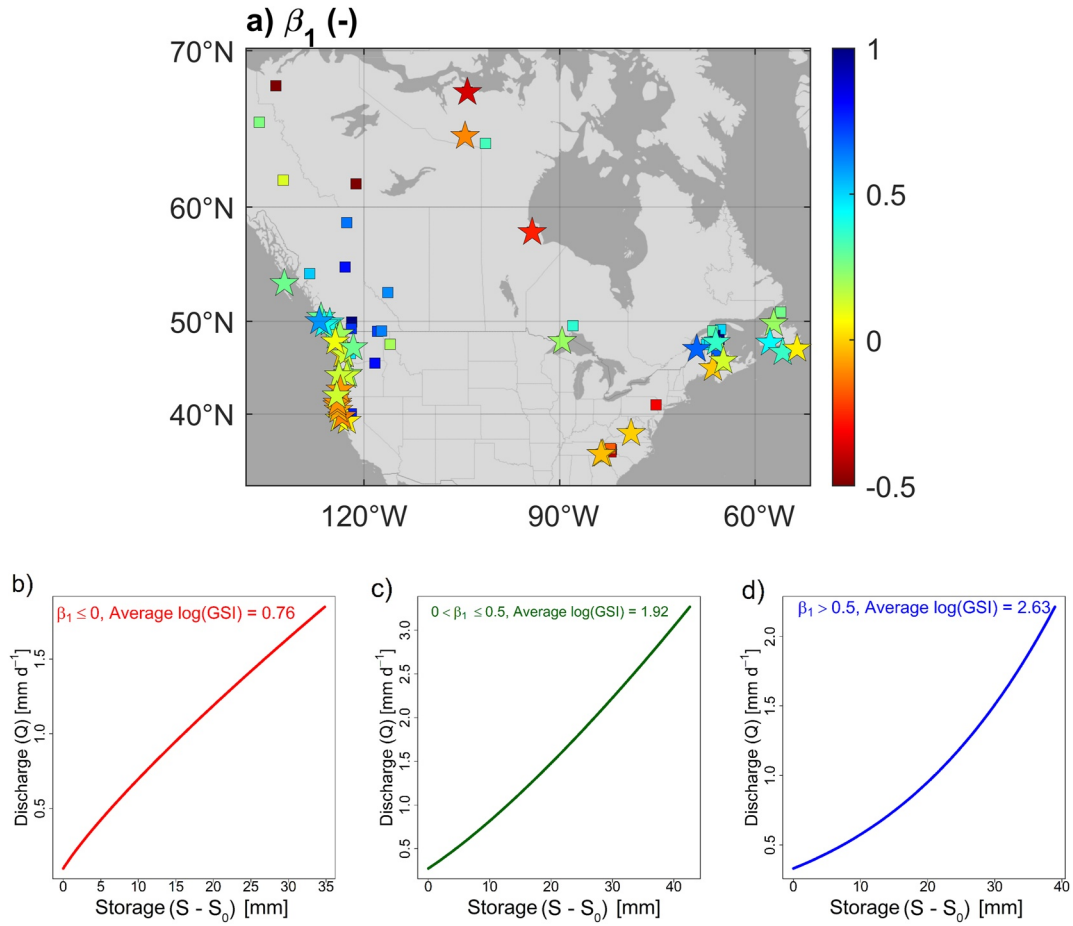

Figure 5. The spatial map of β_1, and the ensembles of low-flow storage–discharge relations for groups of catchments with contrasting β_1 values. (a) The spatial map of β_1 estimated using Base Case method (78 catchments). Stars denote the 37 catchments that were used in both Base Case and Bootstrap analyses. Note that both Base Case and Bootstrap methods estimated identical β_1 values at these 37 catchments. Squares denote the catchments that were only used in Base Case analysis. The ensembles of low-flow storage–discharge relations for groups of catchments with (b) $\beta_1 \leq 0$ (concave storage–discharge), (c) $0 < \beta_1 \leq 0.5$ (slightly convex storage–discharge), and (d) $\beta_1 \geq 0.5$ (convex storage–discharge). The median values of Log GSI are 0.76, 1.92, and 2.63, respectively, for these three groups. Note that storage and discharge represent horizontal axes and vertical axes, respectively, in storage–discharge plot.

Supporting Information S1). Generally, ETS, Base Case, and M25E methods estimate a wider range of β_1 values than M7D and Bootstrap methods. This can be related to more restricted criteria and filters used in M7D and Bootstrap methods in selecting acceptable events or in excluding catchments with a large event-to-event variation, leading to a smaller number of catchments remaining for estimating β_1 in M7D and Bootstrap analyses. It is important to note that most of arid catchments, located in central USA and Canada as well as in southern USA, did not pass the growing season ET/Q < 2 filter and were excluded from all six methods' analyses (Figure 5).

Figure 5a shows the spatial pattern of β_1 estimated using Base Case and Bootstrap methods. Note that all catchments that passed the Bootstrap method's filters (shown by stars in Figure 5a) also passed the Base Case method filters. Additionally, at these catchments, both Base Case and Bootstrap methods estimated almost identical β_1 values. Among the catchments used in the Base Case analysis, the estimated values of β_1 are on average higher in British Columbia, Ontario, Quebec, Nova Scotia, and Newfoundland (all in Canada) than in other regions (Figure 5a). Most of the catchments south of 42°N have β_1 values close to (or lower than) zero (Figure 5a).

4.3. Empirical Analysis: Groundwater Subsidy Index

The distribution of GSI (Equation 6) shows a large spatial variability of this index across our 1,137 study catchments (Figure 6). Catchments located on Canada's West Coast, Rocky Mountains, and the Northwest of the

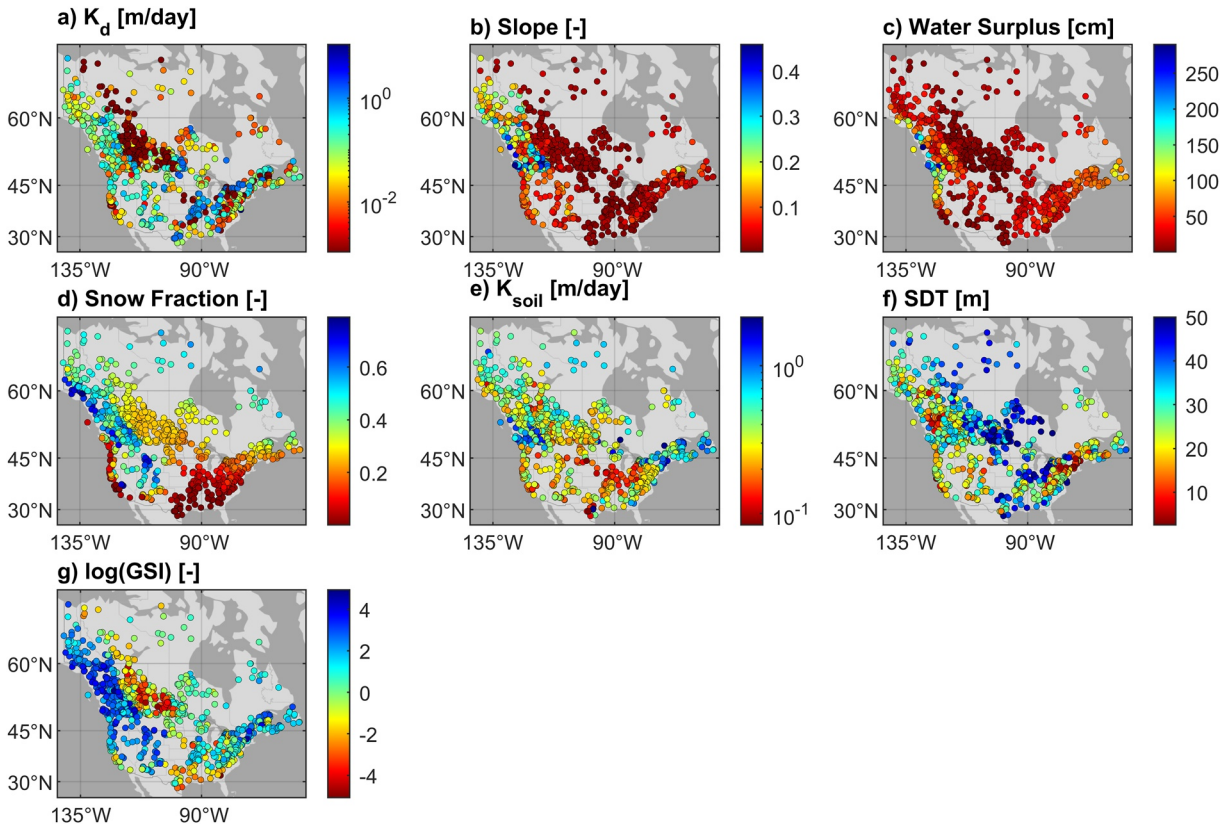

Figure 6. The spatial patterns of individual components of Groundwater Subsidy Index (GSI; a–f) and log GSI (g) along 1,137 study catchments. GSI's components include catchment-scale average slope (S [–]), hydraulic conductivities of soil (K_{soil} [L/T]) and deep geological formation (K_d [L/T]), riparian sedimentary deposit thickness (SDT [L]), water surplus (WS [L]), and snow fraction (SF [–]). Equation 6 was used to calculate GSI from its components (Section 3.4). The references to the source data and the algorithms used to calculate catchment-scale average values of all six components were discussed in Sections 2.2–2.4.

United States exhibit the highest values of GSI on average (Figure 6g). High to moderate GSI values generally appear in Canada's East Coast and the Northeast of the United States. The lowest GSI values are found in the Gulf Coast of the United States and the western provinces of Canadian Prairie. The spatial variability of GSI is the result of the spatial variabilities of all of its components. Indeed, GSI and the scientific concept it conveys are not disproportionately explained by the climatic components or slope but rather explained as a result of the interaction among climatic, topographical, and geological components. The Spearman correlations between GSI and its components across the study catchments are 0.71 (GSI vs. K_d/K_{soil}), 0.69 (GSI vs. S), 0.68 (GSI vs. WS), 0.47 (GSI vs. SF), and −0.34 (GSI vs. SDT). The Spearman correlations among the individual components that make up GSI are generally much smaller. A total of 20 pair correlations are between −0.20 and 0.20, except for S versus WS (with $\rho = 0.56$) and SF versus SDT ($\rho = 0.47$). The weak rank correlations among these individual components that make up GSI, despite the relatively large correlations between GSI and its components, may suggest that each component of GSI, including (surficial) geological attributes, shares a large amount of independent information with GSI. Therefore, a robust explanation of GSI requires the inclusion of all components as each component defines a unique and independent dimension of the whole concept that the GSI conveys.

The individual components of GSI have distinct spatial patterns. The hydraulic conductivity of deep geological formation is distinctively lower in the Prairie Provinces of Canada compared to other regions (Figure 6a). The catchment average slope is significantly higher at the Canada's West Coast and the Canadian portion of Rocky Mountains compared to other regions (Figure 6b). Values of water surplus are the largest along the Canada's West Coast and the Northwest of the United States. Water surplus decreases to the lowest values toward the central part of the continent (e.g., Prairie Provinces of Canada and USA; Figure 6c). Snow fraction generally increases from south to north, with the exception that catchments in major mountain ranges (e.g., Rocky Mountains) have higher snow fraction values compared to other catchments of the similar latitude (Figure 6d). Highly conductive

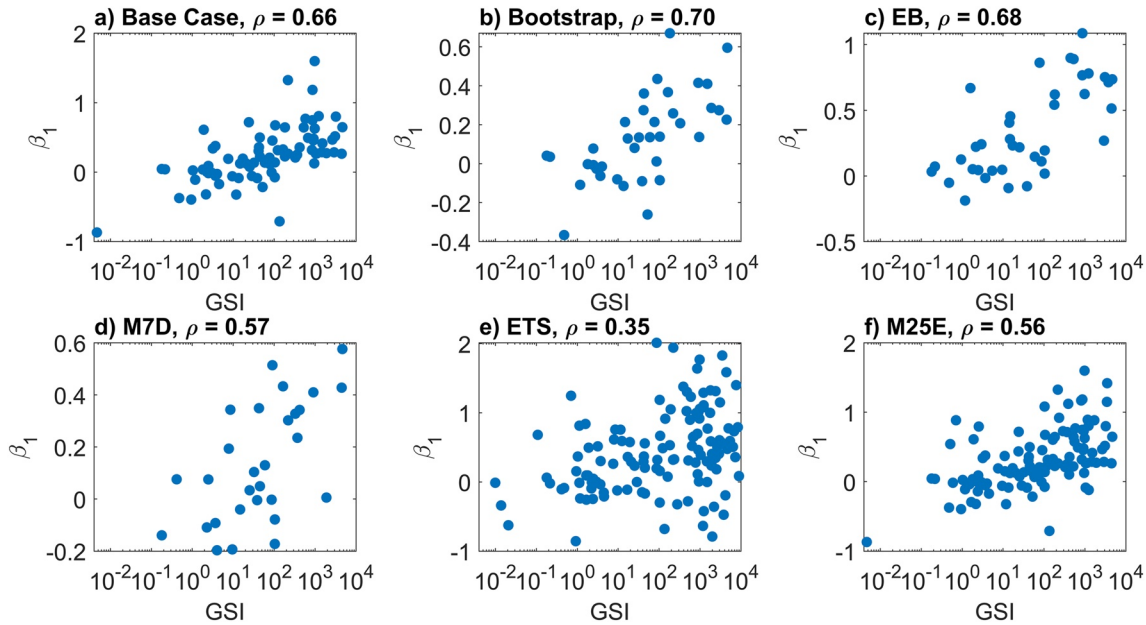

Figure 7. The scatter plots and Spearman (nonlinear) correlation coefficients (ρ') between β_1 and Groundwater Subsidy Index (GSI) using six different methodologies used to estimate β_1. See the description of the Base Case method in Section 3.3. The descriptions of other five methods are in Text S2 in Supporting Information S1. In each methodological variant, only one aspect of the Base Case scenario is modified at a time. For example, EB method uses Equal Binning (instead of quantile binning) to bin the data and ETS uses exponential time step (instead of constant time step) to calculate recession rate. Note that *x*-axes in all figures are in log scale; hence, our plots show that there is a nonlinear association between β_1 and GSI.

soils are found in South Eastern and South Western of Canada (Figure 6e). Catchments with large values of SDT are found in Prairie Provinces of Canada, Canadian territories, and Gulf Coast of the United States (Figure 6f).

4.4. Empirical Analysis: The Spatial Association Between GSI and β_1

The positive (nonlinear) spatial associations between GSI and β_1 are evident with all methodological scenarios used to estimate β_1 (Figure 7). This positive spatial association is strong for Base Case ($\rho' = 0.66$), Bootstrap ($\rho' = 0.70$), and EB ($\rho' = 0.68$) and is moderately strong for M7D ($\rho' = 0.57$) and M25D ($\rho' = 0.56$). The positive spatial association for ETS ($\rho' = 0.35$) is not as strong as other methods. This might be due to smoothening of the late-recession pattern, which may happen in some catchments when using ETS method, as discussed in Text S2 in Supporting Information S1. The spatial association between GSI and β_1 is stronger than the spatial association between each component of GSI and β_1, regardless of the method used to estimate β_1 (Table S3 in Supporting Information S1). This implies that none of GSI's components could explain β_1 as strongly as GSI. Indeed, β_1 is strongly associated with the way the individual components interact together rather than with the individual component alone. For example, for Bootstrap analysis, GSI's association with β_1 ($\rho' = 0.70$) is larger than water surplus's association with β_1 ($\rho' = 0.59$), slope's association with β_1 ($\rho' = 0.43$), and K_d/K_{soil} association with β_1 ($\rho' = 0.42$). Additionally, Table S2 in Supporting Information S1 suggests that two alternative indices of groundwater subsidy (i.e., I_1, I_2), that used GSI's components but did not acknowledge the domain knowledge in the way that GSI did, cannot have associations with β_1 as strong as GSI.

Likewise, GSI is associated with the nonlinearity of storage–discharge relation ($1 - \beta_1$), which reflects the concavity versus convexity of low-flow storage–discharge relation, where storage and discharge represent horizontal axes and vertical axes, respectively. The median GSI value for the group of catchments with β_1 less than zero (or $1 - \beta_1 > 1$) is pronouncedly smaller than the median GSI value for the group of catchments with β_1 larger than 0.5 (or $1 - \beta_1 < 0.5$; Figures 5b–5d). For the group of catchments with $\beta_1 \leq 0$, log GSI has a median value of 0.76, and the ensemble of storage–discharge relation is concave (Figure 5b). Among the catchments used in the Base Case analysis, those located south of 42°N and some catchments in Canadian territories are the member of this group (Figure 5a) with concave storage–discharge relation. Where $0 < \beta_1 \leq 0.5$, log GSI has a median value of 1.92, and the ensemble of storage–discharge relation is convex but very close to linear (Figure 5c). Among

the catchments used in the Base Case analysis, those catchments located in the province of Newfoundland and Labrador of Canada, in addition to a few catchments in other locations (shown in yellow, green, and light blue; Figure 5a) are all the member of this group. For the group of catchments with $\beta_1 > 0.5$, log GSI has a median value of 2.63, and the ensemble of storage–discharge relation of this group is more convex than the previous groups (Figure 5d).

5. Discussion

The influence of deep slow-moving aquifer (e.g., bedrock) connecting upland hillslope groundwater to mainstream—as an additional storage unit beyond that of shallow soil mantled aquifer—remained as a source of uncertainty for both low-flow storage–discharge relation and plant water use (Hahm et al., 2022; Rempe & Dietrich, 2018). Site-specific experimental analysis in intensively monitored sites suggested that upland hillslope groundwater subsidy through bedrock may contribute to low flow's active and total storages and ultimately to low-flow storage–discharge relation (Gabrielli et al., 2018; Hale et al., 2016). However, the extent of upland hillslope groundwater subsidy, and its influence on low-flow storage–discharge relation, varies from one catchment to the other (Gabrielli et al., 2018; Hale et al., 2016), depending on how the catchment climatic and physical attributes interact together (Ameli et al., 2018). In this paper, we focused on developing a quantitative framework and a similarity index to determine the extent of upland hillslope groundwater subsidy. The aim was to explore theoretically and empirically our overarching hypothesis over a wide range of catchment's climatic and physical settings. Our hypothesis was that a larger extent of upland hillslope groundwater subsidy through deep slow-moving aquifer (e.g., bedrock), relative to groundwater contribution through shallow riparian sedimentary deposit aquifer, increases the nonlinearity of sensitivity function (β_1) and the convexity of low-flow storage–discharge relation from one catchment to the other. We discuss the findings of our hypothesis testing in Section 5.1. We also discuss the potential cause of the deviation in estimated β_1 values in our empirical analysis from the range of values suggested by Boussinesq-based hydraulic groundwater theory (Section 5.2). The implications of our findings for evaluating drought vulnerability of landscapes in different climatic and physical settings as well as for assessing groundwater age and stream transit times are discussed in Sections 5.3 and 5.4. The limitations of our study and future directions will be discussed in Section 5.5.

5.1. Upland Hillslope Groundwater Subsidy Affects the Nonlinearity of Sensitivity Function and the Convexity (Shape) of Low-Flow Storage–Discharge Relation

Our theoretical analysis depicts that β_1 generally increases, and the shape of low-flow storage–discharge relation varies from relatively concave to convex, with an increase in the ratio of groundwater contribution from deep slow-moving reservoir relative to shallow fast-moving reservoir (which is equivalent to an increase in $T_d \times i_d / T_s \times i_s$, θ_d/θ_s, and/or α_d/α_s; Figure 4). Such influence is particularly strong where $T_d \times i_d / T_s \times i_s$ is above a certain threshold. These theoretical influences on β_1 can be attributed to the fact that the differences between the transmission timescales of linear reservoirs of a multilinear reservoir system control the nonlinear function that relates the system's storage to the system's discharge (Harman et al., 2009). In our case, the transmission timescale ratio of deep slow-moving to shallow fast-moving reservoirs (i.e. τ_d/τ_s) could control β_1. The catchment's β_1 is large where the relative contribution of deep slow-moving reservoir, with a long transmission timescale, is large, which leads to distinct transmission timescales of deep slow-moving and shallow fast-moving reservoirs ($\tau_d/\tau_s \gg 1$). On the other hand, for the catchment with a minimal contribution of deep slow-moving reservoir to low-flow discharge, one uniform transmission time-scale could explain the late-recession dynamics, leading to a small value of catchment's β_1 (e.g., $\beta_1 < 0.5$ as shown by dashed line in Figure 4). Conceptually, these findings imply that the long tail of late recession or the significant convexity of low-flow storage–discharge relation (see Figures 3b′ and 3b″) is controlled by the extent of delayed groundwater contribution and can be sufficiently explained if (at least) one additional reservoir with a long transmission timescale being added to the existing fast-moving reservoir.

Overall, our theoretical analysis suggests that the relative extent of deep slow-moving groundwater contribution—which is assumed to connect upland hillslope groundwater subsidy to stream in our study—increases the nonlinearity of sensitivity function and the convexity of low-flow storage–discharge relation. Our empirical analysis further verifies the theoretical finding. As GSI increases among catchments, the typical nonlinearity of low-flow sensitivity function and the convexity of low-flow storage–discharge increase (Figures 6b–6d and 7). Our findings

are consistent with the qualitative synthesis made by Wlostowski et al. (2021) across 15 USA-CZO sites. They concluded that large deep groundwater transmission from uplands through permeable hillslope bedrock leads to a low sensitivity to subsurface storage (or potentially large β_1). In contrast, they demonstrated that the dominancy of fast and transient lateral water movement in the shallow soil, with a reduced recharge to deep aquifer, leads to a high stream low-flow sensitivity to subsurface storage (or potentially small β_1). Additionally, Tague and Grant (2004) experimental analysis at Willamette River Basin in Oregon showed that catchments with damped stream response at low flow (i.e., large β_1) are those with high ridgeline bedrock water table and large active bedrock storage and large bedrock hydraulic gradient (see Figure 3b for the conceptualization of such catchments), and greater volume of bedrock old water contributing to low flow.

5.2. To What Extent Does Hydraulic Groundwater Theory Explain the Nonlinearity of Sensitivity Function and the Convexity of Low-Flow Storage–Discharge Relation?

Boussinesq-based hydraulic groundwater theory assumes that the catchment-scale storage–discharge relation follows that of a "representative" storage unit (or aquifer) whose hydraulic property (e.g., transmission timescale) is representative of the hydraulic properties of the collection of storage units (e.g., bedrock aquifer, riparian sedimentary deposit aquifer) that make up a catchment. For example, this theory suggests that if one single horizontal unconfined aquifer, with an inverse incomplete Beta function as the initial condition, sufficiently represents the hydraulic properties of the collection of storage units that make up a catchment, the catchment's low-flow storage–discharge behavior may reveal a nonlinearity of $\beta_1 = 0.5$ (or $b_1 = 1.5$). As another example, Harman and Sivapalan (2009) analytically showed that if a thin unconfined aquifer sufficiently represents the catchment's low-flow storage–discharge behavior (similar to Figure 3a), we may expect to see a catchment's β_1 smaller than zero ($-1 < \beta_1 < 0$). While no continuous relationship was developed between β_1 and hydrologically relevant catchment critical zone attributes before, hydraulic groundwater theory suggested a range of β_1 between -1 and 0.5 (or a range of b_1 between 0 and 1.5) for different topography, geomorphology, geology, climate, and initial condition of the representative storage unit (see the review paper by Troch et al. (2013)).

The β_1 range suggested by hydraulic groundwater theory could explain the low-flow dynamics of a large portion (but not all) of the catchments assessed in our empirical analysis (Figure 6a). In the Base Case analysis, the third quantile of the estimated β_1 is 0.47 and the maximum estimated value is 1.60 (Table S1 in Supporting Information S1). Bootstrap analysis, which selects only the catchments with minimal event-to-event variation at late recession (see Text S2 in Supporting Information S1), leads to a smaller third quantile of estimated β_1 (equals to 0.27) and a smaller maximum of estimated β_1 (equals to 0.67; Table S1 in Supporting Information S1). In another empirical analysis, Wittenberg (1999) showed that the nonlinearity of storage–discharge relation dominating low flow ($1 - \beta_1$ in Equation 3) could vary between 0 and 1.1 (or β_1 varies between -0.1 and 1) along 80 catchments in Germany. The possibility of smaller than 0.5 (and negative) β_1, or relatively concave storage–discharge relation dominating low flow, suggested by hydraulic groundwater theory, and estimated by the empirical study across Germany as well as our empirical analysis, may suggest that hydraulic groundwater theory might be sufficient to explain the nonlinearity of low-flow dynamics in a large portion of catchments. This is particularly true for the majority of catchments with a temporally stable relationship between $\log(g(Q))$ and $\log(Q)$ (i.e., minimal event-to-event deviation from a typical β_1). Kim et al. (2023) data-guided analysis in a single catchment study also depicted the validity of the Boussinesq model in explaining the late-recession flow dynamics. They showed that despite large event-to-event variability at early recession, during the late recession, the nonlinearity of events' trajectories converges to a typical (or central tendency) nonlinearity that is not far from the one estimated by the Boussinesq model.

Our theoretical analysis suggests that the catchments with small β_1 are those with a relatively small groundwater subsidy through deep slow-moving reservoir (showed by $T_d \times i_d / T_s \times i_s < 0.5$ and $\theta_d/\theta_s < 0.33$ and $\alpha_d/\alpha_s < 10$; Figure 4). Our empirical analysis depicts that the catchments with estimated β_1 values within the proposed range by hydraulic groundwater theory (i.e., $\beta_1 < 0.5$) have a relatively small groundwater subsidy from upland hillslopes, with GSI values smaller than 10 and smaller than 50 for Base Case and Bootstrap analyses, respectively (note that GSI can be as large as 5,000 among our study catchments; Figure 7). These findings are consistent with that of Wittenberg (1999) who conceptually related the values of β_1 smaller than 0.5 to relatively large storage capacity of shallow riparian aquifer (or relatively large H_s and T_s, see Figure 3a) and/or predominantly fast shallow subsurface flow such as macropores and subsurface stormflow within shallow soil mantled aquifer, with a reduced recharge into hillslopes deep slow-moving aquifer. Overall our theoretical and empirical findings,

and that of existing literature mentioned above, may suggest that hydraulic groundwater theory could explain the low-flow storage–discharge functionality in catchments with a relatively small (but still not negligible) extent of deep slow-moving groundwater subsidy sourced from upland hillslopes. One may conclude that in these catchments as the contribution from the deep slow-moving aquifer is relatively small, one single representative storage unit (or a [non]linear reservoir) might be sufficient to represent the low-flow-related hydraulic properties of the collection of storage units that make up the catchment. Building on GSI definition (see Section 3.4), these catchments may have a small slope and/or small recharge into deep slow-moving aquifer (i.e., small $\frac{WS \times S}{K_{soil}/K_d}$).

However, hydraulic groundwater theory does not explain the entire range of estimated β_1 in the empirical analysis of multiple studies, including ours. Wittenberg's range of estimated β_1 (−0.1 to 1) across Germany, Tague and Grant (2004) range of estimated β_1 (0 to 2) across Willamette River Basin in Oregon, and the estimated β_1 range in our empirical analysis (e.g., −0.87 to 1.6 for Base Case or −0.86 to 2.01 for ETS, see Table S1 in Supporting Information S1) go beyond the Boussinesq-based theoretical range (i.e., $-1 < \beta_1 < 0.5$). Wittenberg (1999) and Chapman (1999) related β_1 larger than 0.5 to large convergence of groundwater flow from hillslope toward riparian zone (which is equivalent to large i_d/i_s and H_d/H_s, see Figure 3b). Our theoretical analysis suggests that the catchments with a relatively large β_1 have $T_d \times i_d/T_s \times i_s > 0.5$ and $\alpha_h/\alpha_r > 10$ or $\theta_d/\theta_s > 0.33$ (Figure 4). Moreover, our empirical analysis shows that catchments with β_1 value larger than 0.5 generally have large GSI values (larger than 10 and up to 5,000; Figure 7). It can be inferred where groundwater subsidy from upland hillslope becomes distinctly large, one single representative storage unit (or [non]linear reservoir) might not be sufficient to represent the hydraulic properties of the collection of storage units that make up the catchment. One potential explanation of β_1 values larger than 0.5 in these catchments is the existence of two distinct representative storage units, with distinct transmission timescales. One representative storage unit with short transmission timescale represents the hydraulic properties of the collection of fast-moving storage units (e.g., shallow riparian sedimentary deposit aquifers), and the second representative storage unit with long transmission timescale represents the hydraulic properties of the collection of slow-moving storage units (e.g., bedrock aquifer that connects the upland hillslope groundwater to mainstream). Expanding on GSI definition (see Section 3.4), these catchments may have large slopes and/or large recharges into deep slow-moving aquifer (i.e., large $\frac{WS \times S}{K_{soil}/K_d}$).

Similar to the conclusions made by the theoretical analysis of Harman et al. (2009) and empirical analysis by Tashie, Pavelsky, and Emanuel (2020) on the nonlinearity of the overall recession, the findings in our study may raise a new hypothesis regarding the late-recession dynamics and nonlinearity. This hypothesis suggests that in catchments with a strong influence of secondary storage unit (with distinct hydraulic property than the primary storage unit), the current state of hydraulic groundwater theory, using one single representative storage unit, may not be able to sufficiently explain the long tail of late recession or a large convexity of low-flow storage–discharge relation. This hypothesis should be further explored in the future studies.

5.3. Groundwater Subsidy Index as a New Descriptor of Catchment Drought Vulnerability

Identifying the vulnerability of stream low flow in ungauged regions is a highly important goal. Tashie et al. (2020) related the nonlinearity of a catchment sensitivity function at low flow to the drought resistance of the catchment (i.e., larger β_1 implies a more persistent nonzero low-flow events; as conceptualized in our Figure 3). Larger estimated β_1 along the Canada's West Coast may suggest a higher drought resistance of these landscapes with convex storage–discharge relation, compared to highly draught vulnerable catchments located south of 42°N with a relatively concave storage–discharge relation and a relatively small estimated β_1 (Figure 5). However, the prediction of the nonlinearity of catchment sensitivity function in ungauged regions is challenging and available (machine learning) models fall short in this regard. As an example, H. Li and Ameli (2022) developed a Random Forest model with 18 predictors for predicting the nonlinearity of sensitivity function in ungauged regions and could not get an acceptable prediction accuracy ($R^2 \sim 40\%$). The large association between our proposed GSI and β_1 may suggest that GSI—which was developed independent of streamflow observations and based on hydrologically relevant interactions among critical zone attributes with globally available data—could be considered as a catchment drought vulnerability indicator in future regionalization practices and climate change impact assessment analyses.

5.4. Groundwater Subsidy Index as a Potential Descriptor of Stream Transit Time at Low Flow

A large catchment's GSI generally reflects a relatively large groundwater contribution through deep slow-moving aquifer compared to shallower fast-moving aquifer. Deep slow-moving aquifer typically releases groundwater

with an old age. This may raise the hypothesis that in catchments with a large GSI, large contribution of old groundwater to low flow may override young groundwater contributions from shallower and faster compartments, leading to a disproportionately old stream low-flow transit time. At a wet and relatively permeable Scottish catchment (with potentially large GSI), Birkel et al. (2015) showed that large contributions of upland hillslopes old groundwater disproportionately influence stream low-flow transit time. Later, Hale et al. (2016), by comparing 15 nested research catchments in western Oregon, showed that catchments with permeable (fractured and weathered) sandstone bedrock reveal a much longer stream transit time than those with tight volcanic low-permeable bedrock (everything else including, topography, climate, and land cover were similar among all 15 catchments). The former catchments, with potentially larger GSI, displayed an average of 6.2 years stream transit time, while the latter catchments, with potentially smaller GSI, showed an average of 1.8 years stream transit time. These experimental studies along with our empirical analysis' findings may suggest that an index that explains the relative extent of groundwater contribution from deep slow-moving aquifer may inform stream low-flow transit time. Additionally, as discussed by Gabrielli et al. (2018)—and building on the previous studies' findings on the lack of association between individual critical zone attribute (e.g., slope) and stream transit time (cf., Hale et al., 2016)—an index able to explain the stream transit time should incorporate the hydrologically relevant interactions among catchment critical zone attributes. Our proposed GSI has both aforementioned characteristics and thus might be a good candidate to be used for comparing stream low-flow transit time among catchments. Hence, future work could explore the applicability of our GSI or similarly developed indices in explaining variations in stream transit time among catchments.

5.5. Limitations of the Study and Future Research Directions

5.5.1. The Use of Two Linear Reservoirs in Parallel in the Theoretical Analysis

Similar to Clark et al. (2009) and Roques et al. (2022), by assuming reservoirs in parallel, our theoretical analysis neglects the interactions between the two representative storage units (light blue arrows in Figure 3 reflect such an interaction). Where the vertical (downgradient) flow along the hillslopes' bedrock is dominant, during low-flow condition, such an interaction might be minimal and shallow and deep units may independently contribute groundwater to stream. For example, Gabrielli et al. (2018) at the Maimai catchment measured the vertical bedrock flow and indicated that, while both storage units contribute groundwater to low flow, the groundwater age of shallow riparian aquifer (∼4 months) and deep slow-moving (or bedrock) aquifer (∼23 years) is distinctively different at their discharge point. This shows a minimal water particle exchange (or velocity and water age independence) between deep slow-moving and shallow fast-moving aquifers. Although water age independence may not necessarily indicate the celerity (or excess energy propagation) independence between the two aquifers, such a significant water age difference may suggest that two distinct groundwater systems with distinct celerity patterns generate the Maimai's low flow. Otherwise, if excess energy was being strongly propagated between the two storages (or both storages were part of one single groundwater system), we may have seen a relatively larger mixture of the old and younger particles. The interaction between the two storages, however, can be large where deep slow-moving aquifer (e.g., bedrock) exfiltrates shallow fast-moving riparian sedimentary deposit aquifer far away from the mainstream. Future works may consider a more complex reservoir system to incorporate both in-parallel (independent) and in-series (interacting) contributions from the reservoirs to theoretically explore more diverse mechanisms of low-flow dynamics.

The use of a linear reservoir to emulate the behavior of each storage unit might be a simplified representation of storage–discharge behavior. On one hand, the hydraulic of groundwater discharge from the representative shallow riparian fast-moving storage unit only under certain circumstances could be presented by a linear reservoir (Wittenberg, 1999). On the other hand, the hydraulic properties of upland hillslopes could be variable among hillslopes and the use of one linear reservoir could neglect the (potentially large) variability of transmission characteristics among hillslopes (Ranjram & Craig, 2022). Such a simplified treatment, however, allowed us to explore our overarching hypothesis, setting the stage for more realistic theoretical analyses in future works (e.g., the use of two nonlinear reservoirs or multiple (more than two) linear reservoirs).

The closed form equation obtained as the result of theoretical analysis (Equation 5) is valid under the assumptions and approximation stated in Section 3.2. The equation provides progress in linking β_1 to a catchment's hydraulic characteristics in a nonlinear manner. This equation allows β_1 to vary continuously depending on catchment's hydraulic characteristics across a large range, as opposed to previous studies' findings which led to only certain

discrete values for β_1 (or b_1), varying across a small range (see discussion in Section 5.2). Our empirical analysis further clarified that certain discrete values for β_1 (or b_1), varying across a small range, cannot thoroughly explain observed values and ranges of β_1 (or b_1). Future research could build on Equation 5 and relax their assumptions and approximation to obtain a more realistic (and probably more nonlinear) analytical equation linking β_1 (or b_1) to the catchment's hydraulic characteristics.

5.5.2. Exclusion of Most of Dry Catchments

Catchment and event selection criteria and filters, explained in Section 3.3, excluded most of dry catchments (with aridity index larger than 1.5) in central North America and southern USA from our empirical analysis. Particularly, large evapotranspiration during growing season in these regions could limit understanding of low-flow generation processes from sensitivity function estimation. As daily-scale evapotranspiration is not much less than streamflow during growing season, little (or no) acceptable samples remain for sensitivity function estimation. Although the findings of our theoretical analysis could be generalized to dry catchments, our empirical analysis findings are not generalizable to dry catchments. Accurate and high-resolution (e.g., hourly) data set on evapotranspiration and streamflow can help estimating sensitivity function in arid regions by accurately identifying the sufficient number of recession events with hourly scale evapotranspiration smaller than streamflow (as done by Kirchner, 2009; Teuling et al., 2010), rather than excluding the arid catchments from the analysis.

5.5.3. Uncertainty in GSI Calculation

GSI, which was calculated using globally available data, was intended to estimate the relative groundwater flow contribution from upland hillslope versus riparian aquifer. However, this index can only be used to compare among catchments their relative sources of low flow and cannot estimate the exact value of groundwater contributions from upland hillslope and or from riparian aquifer. As explained in Section 3.4, this shortcoming would not affect the findings of our empirical analysis, given the comparative nature of the analysis. Nonetheless, given the important eco-hydrological and hydro-geochemical implications of these groundwater flow contributions (See Van Meter et al., 2018), future works could focus on developing metrics able to directly quantify these contributions.

In deriving GSI, we leveraged available literature to justify the nonlinear associations between H_d (and i_d/i_s) and critical zone attributes as explained in Section 3.4. These nonlinear associations were incorporated through interactions among critical zone attributes. The importance of the interactions among critical zone attributes in explaining catchment hydrologic functions has been emphasized in the previous data-guided (Janssen & Ameli, 2021) and experimental (Hopp & McDonnell, 2009) studies. However, the associations between H_d (and i_d/i_s) and critical zone attributes and ultimately between GSI and critical zone attributes may take additional nonlinear functional forms (e.g., exponential). While the current version of GSI, derived using interaction function alone, was able to explain a large portion of the spatial variability of β_1, future research could focus on deriving the functional relationship between H_d (and i_d/i_s) and critical zone attributes, which then can be used to derive a potentially more comprehensive version of GSI (or other similar indices used to explain catchment hydrologic functions). Given the importance of the interaction among critical zone attributes showcased in the previous data-guided and experimental studies, we expect that the new functional relationship still includes the interaction functionality and other nonlinear functionalities (if exist) are being added to the interaction term. Hence, the version of GSI derived in our paper could be considered as a simple (but nonlinear) version of a potentially more comprehensive and more nonlinear index which explains the relative ratio of upland hillslope groundwater subsidy to shallow fast-moving riparian groundwater.

5.5.4. Other Relevant Hypotheses Regarding the Nonlinearity of Sensitivity Function and the Shape of Storage–Discharge Relation at Low Flow

We acknowledge that there might be other valid conceptual models able to explain sensitivity function nonlinearity and storage–discharge relation at low-flow condition. Our theoretical analysis suggests that β_1 is generally being controlled by the relative groundwater contributions (and the transmission timescale ratio) of slow-moving reservoir versus fast-moving reservoir. In our paper, we corresponded the slow-moving reservoir to an aquifer connecting upland hillslope groundwater to mainstream. However, there might be geological conditions under which the slow-moving reservoir has nothing to do with the upland hillslopes, and both slow-moving and fast-moving reservoirs, with distinct transmission timescales, occur in the riparian area. Overall, further theoretical and empirical research is needed to better understand diverse conceptual models of low-flow storage–discharge relation in

different environmental settings. This helps to develop a widely applicable and transferrable framework able to estimate low-flow storage–discharge relation in (un)gauged regions, improving our understanding of low-flow generation processes and improving the quality of model development and ultimately assessments of the impacts of global environmental changes on low flow.

6. Conclusion

We demonstrated, both empirically and theoretically, that with an increase in the relative extent of deep slow-moving groundwater subsidy, sourced from upland hillslopes, the nonlinearity of mainstream low-flow sensitivity to storage increased and the shape of low-flow storage–discharge relation altered from relatively concave to convex. The range of nonlinearities proposed by hydraulic groundwater theory could cover the estimated nonlinearities of a large portion of our studied catchments. These catchments typically have a relatively small extent of deep slow-moving groundwater subsidy sourced from upland hillslopes. However, in catchments where the groundwater contribution from upland hillslopes to low-flow discharge becomes distinctly large, relative to the contribution from shallow riparian sedimentary deposit aquifer, hydraulic groundwater theory using one single representative storage unit (or [non]linear reservoir) might not be sufficient to explain the large estimated nonlinearity values (β_1 values larger than 0.5). Our findings on the mechanistic causes of the nonlinearity of low-flow storage–discharge relation could improve (a) our understanding of low-flow generation processes and catchment's hydro-geochemical functions, (b) the estimation of low-flow transit time, and (c) the quality of model development and ultimately assessments of the impacts of global environmental changes on stream low flows.

Data Availability Statement

Gridded climatic data used in our study were obtained from the ERA5-Land database (Muñoz-Sabater et al., 2021). Catchment-scale data used in six methodological variants were published in H. Li and Ameli (2023).

Acknowledgments
This research was funded by the grants awarded to AAA by NSERC-Funded Canadian Statistical Science Institute (CANSSI) and by NSERC Discovery Grants program. We thank the associate editor and three reviewers of *Water Resources Research Journal* for their constructive comments. We also thank Maria Belen Rios Sialer for proof-reading the manuscript.

References

Addor, N., Newman, A. J., Mizukami, N., & Clark, M. P. (2017). The CAMELS data set: Catchment attributes and meteorology for large-sample studies. *Hydrology and Earth System Sciences*, *21*(10), 5293–5313. https://doi.org/10.5194/hess-21-5293-2017

Ajami, H., Troch, P. A., Maddock, T., Meixner, T., & Eastoe, C. (2011). Quantifying mountain block recharge by means of catchment-scale storage–discharge relationships. *Water Resources Research*, *47*, W04504. https://doi.org/10.1029/2010WR009598

Ameli, A. A., Beven, K., Erlandsson, M., Creed, I., McDonnell, J., & Bishop, K. (2017). Primary weathering rates, water transit times, and concentration–discharge relations: A theoretical analysis for the critical zone. *Water Resources Research*, *53*, 942–960. https://doi.org/10.1002/2016WR019448

Ameli, A. A., Craig, J., & McDonnell, J. (2015). Are all runoff processes the same? Numerical experiments comparing a Darcy-Richards solver to an overland flow-based approach for subsurface storm runoff simulation. *Water Resources Research*, *51*, 10008–10028. https://doi.org/10.1002/2015WR017199

Ameli, A. A., & Creed, I. F. (2018). Groundwaters at risk: Wetland loss changes sources, lengthens pathways, and decelerates rejuvenation of groundwater resources. *Journal of the American Water Resources Association*, *55*(2), 294–306. https://doi.org/10.1111/1752-1688.12690

Ameli, A. A., Gabrielli, C. P., Morgenstern, U., & McDonnell, J. (2018). Groundwater subsidy from headwaters to their parent water watershed: A combined field-modeling approach. *Water Resources Research*, *54*, 5110–5125. https://doi.org/10.1029/2017WR022356

Berghuijs, W. R., Hartmann, A., & Woods, R. A. (2016). Streamflow sensitivity to water storage changes across Europe. *Geophysical Research Letters*, *43*, 1980–1987. https://doi.org/10.1002/2016GL067927

Birkel, C., Soulsby, C., & Tetzlaff, D. (2011). Modelling catchment-scale water storage dynamics: Reconciling dynamic storage with tracer-inferred passive storage. *Hydrological Processes*, *25*(25), 3924–3936. https://doi.org/10.1002/hyp.8201

Birkel, C., Soulsby, C., & Tetzlaff, D. (2015). Conceptual modelling to assess how the interplay of hydrological connectivity, catchment storage and tracer dynamics controls nonstationary water age estimates. *Hydrological Processes*, *29*(13), 2956–2969. https://doi.org/10.1002/hyp.10414

Blöschl, G., Sivapalan, M., Wagener, M., Viglione, A., & Savenije, H. (2014). *Runoff prediction in ungauged basins*. Cambridge University Press.

Brooks, P. D., Chorover, J., Fan, Y., Godsey, S. E., Maxwell, R. M., McNamara, J. P., & Tague, C. (2015). Hydrological partitioning in the critical zone: Recent advances and opportunities for developing transferable understanding of water cycle dynamics. *Water Resources Research*, *51*, 6973–6987. https://doi.org/10.1002/2015WR017039

Brutsaert, W., & Nieber, J. L. (1977). Regionalized drought flow hydrographs from a mature glaciated plateau. *Water Resources Research*, *13*(3), 637–643. https://doi.org/10.1029/WR013i003p00637

Buttle, J. M. (2016). Dynamic storage: A potential metric of inter-basin differences in storage properties. *Hydrological Processes*, *30*(24), 4644–4653. https://doi.org/10.1002/hyp.10931

Carrer, G. E., Klaus, J., & Pfister, L. (2019). Assessing the catchment storage function through a dual-storage concept. *Water Resources Research*, *55*, 476–494. https://doi.org/10.1029/2018WR022856

Chapman, T. (1999). A comparison of algorithms for stream flow recession and baseflow separation. *Hydrological Processes*, *13*(5), 701–714.

Clark, M. P., Rupp, D. E., Woods, R. A., Tromp-van Meerveld, H., Peters, N., & Freer, J. (2009). Consistency between hydrological models and field observations: Linking processes at the hillslope scale to hydrological responses at the watershed scale. *Hydrological Processes*, *23*(2), 311–319. https://doi.org/10.1002/hyp.7154

Condon, L. E., Markovich, K. H., Kelleher, C. A., McDonnell, J. J., Ferguson, G., & McIntosh, J. C. (2020). Where is the bottom of a watershed? *Water Resources Research*, *56*, e2019WR026010. https://doi.org/10.1029/2019WR026010

Cooper, M. G., Zhou, T., Bennett, K. E., Bolton, W., Coon, E., Fleming, S. W., et al. (2023). Detecting permafrost active layer thickness change from nonlinear baseflow recession. *Water Resources Research*, *59*, e2022WR033154. https://doi.org/10.1029/2022WR033154

Dai, Y., Xin, Q., Wei, N., Zhang, Y., Shangguan, W., Yuan, H., et al. (2019). A global high-resolution data set of soil hydraulic and thermal properties for land surface modeling. *Journal of Advances in Modeling Earth Systems*, *11*, 2996–3023. https://doi.org/10.1029/2019MS001784

Gabrielli, C., Morgenstern, U., Stewart, M., & McDonnell, J. (2018). Contrasting groundwater and streamflow ages at the Maimai watershed. *Water Resources Research*, *54*, 3937–3957. https://doi.org/10.1029/2017WR021825

Gao, M., Chen, X., Liu, J., Zhang, Z., & Cheng, Q.-b. (2017). Using two parallel linear reservoirs to express multiple relations of power-law recession curves. *Journal of Hydrologic Engineering*, *22*(7), 04017013. https://doi.org/10.1061/(ASCE)HE.1943-5584.0001518

Grant, G. E., & Dietrich, W. E. (2017). The frontier beneath our feet. *Water Resources Research*, *53*, 2605–2609. https://doi.org/10.1002/2017WR020835

Hahm, W. J., Dralle, D. N., Sanders, M., Bryk, A. B., Fauria, K. E., Huang, M.-H., et al. (2022). Bedrock vadose zone storage dynamics under extreme drought: Consequences for plant water availability, recharge, and runoff. *Water Resources Research*, *58*, e2021WR031781. https://doi.org/10.1029/2021WR031781

Hale, V. C., McDonnell, J. J., Stewart, M. K., Solomon, D. K., Doolitte, J., Ice, G. G., & Pack, R. T. (2016). Effect of bedrock permeability on stream base flow mean transit time scaling relationships: 2. Process study of storage and release. *Water Resources Research*, *52*, 1375–1397. https://doi.org/10.1002/2015WR017660

Harman, C., & Sivapalan, M. (2009). A similarity framework to assess controls on shallow subsurface flow dynamics in hillslopes. *Water Resources Research*, *45*, W01417. https://doi.org/10.1029/2008WR007067

Harman, C., Sivapalan, M., & Kumar, P. (2009). Power law catchment-scale recessions arising from heterogeneous linear small-scale dynamics. *Water Resources Research*, *45*, W09404. https://doi.org/10.1029/2008WR007392

Hopp, L., & McDonnell, J. J. (2009). Connectivity at the hillslope scale: Identifying interactions between storm size, bedrock permeability, slope angle and soil depth. *Journal of Hydrology*, *376*(3–4), 378–391. https://doi.org/10.1016/j.jhydrol.2009.07.047

Hrachowitz, M., Savenije, H., Blöschl, G., McDonnell, J., Sivapalan, M., Pomeroy, J., et al. (2013). A decade of Predictions in Ungauged Basins (PUB)—A review. *Hydrological Sciences Journal*, *58*(6), 1198–1255. https://doi.org/10.1080/02626667.2013.803183

Huscroft, J., Gleeson, T., Hartmann, J., & Börker, J. (2018). Compiling and mapping global permeability of the unconsolidated and consolidated Earth: GLobal HYdrogeology MaPS 2.0 (GLHYMPS 2.0). *Geophysical Research Letters*, *45*, 1897–1904. https://doi.org/10.1002/2017GL075860

Janssen, J., & Ameli, A. A. (2021). A hydrologic functional approach for improving large-sample hydrology performance in poorly gauged regions. *Water Resources Research*, *57*, e2021WR030263. https://doi.org/10.1029/2021WR030263

Kim, M., Bauser, H. H., Beven, K. J., & Troch, P. A. (2023). Time-variability of flow recession dynamics: Application of machine learning and learning from the machine. *Water Resources Research*, *59*, e2022WR032690. https://doi.org/10.1029/2022WR032690

Kirchner, J. W. (2009). Catchments as simple dynamical systems: Catchment characterization, rainfall-runoff modeling, and doing hydrology backward. *Water Resources Research*, *45*, W02429. https://doi.org/10.1029/2008WR006912

Klaus, J., McDonnell, J., Jackson, C., Du, E., & Griffiths, N. A. (2015). Where does streamwater come from in low-relief forested watersheds? A dual-isotope approach. *Hydrology and Earth System Sciences*, *19*(1), 125–135. https://doi.org/10.5194/hess-19-125-2015

Li, H., & Ameli, A. A. (2022). A statistical approach for identifying factors governing streamflow recession behaviour. *Hydrological Processes*, *36*(10), e14718. https://doi.org/10.1002/hyp.14718

Li, H., & Ameli, A. A. (2023). Upland hillslope groundwater subsidy affects low-flow storage–discharge relationship [Dataset]. Zenodo. https://doi.org/10.5281/zenodo.8287450

Li, L., Maher, K., Navarre-Sitchler, A., Druhan, J., Meile, C., Lawrence, C., et al. (2017). Expanding the role of reactive transport models in critical zone processes. *Earth-Science Reviews*, *165*, 280–301. https://doi.org/10.1016/j.earscirev.2016.09.001

Li, L., Stewart, B., Zhi, W., Sadayappan, K., Ramesh, S., Kerins, D., et al. (2022). Climate controls on river chemistry. *Earth's Future*, *10*, e2021EF002603. https://doi.org/10.1029/2021EF002603

Lu, J., Wang, G., Chen, T., Li, S., Hagan, D. F. T., Kattel, G., et al. (2021). A harmonized global land evaporation dataset from model-based products covering 1980–2017. *Earth System Science Data*, *13*(12), 5879–5898. https://doi.org/10.5194/essd-13-5879-2021

Markovich, K. H., Manning, A. H., Condon, L. E., & McIntosh, J. C. (2019). Mountain-block recharge: A review of current understanding. *Water Resources Research*, *55*, 8278–8304. https://doi.org/10.1029/2019WR025676

Martens, B., Schumacher, D. L., Wouters, H., Muñoz-Sabater, J., Verhoest, N. E., & Miralles, D. G. (2020). Evaluating the land-surface energy partitioning in ERA5. *Geoscientific Model Development*, *13*(9), 4159–4181. https://doi.org/10.5194/gmd-13-4159-2020

McDonnell, J. J. (2017). Beyond the water balance. *Nature Geoscience*, *10*(6), 396. https://doi.org/10.1038/ngeo2964

Muñoz-Sabater, J., Dutra, E., Agustí-Panareda, A., Albergel, C., Arduini, G., Balsamo, G., et al. (2021). ERA5-Land: A state-of-the-art global reanalysis dataset for land applications [Dataset]. *Earth System Science Data Discussions*, *13*(9), 4349–4383. https://doi.org/10.5194/essd-13-4349-2021

Pelletier, J. D., Broxton, P. D., Hazenberg, P., Zeng, X., Troch, P. A., Niu, G. Y., et al. (2016). A gridded global data set of soil, intact regolith, and sedimentary deposit thicknesses for regional and global land surface modeling. *Journal of Advances in Modeling Earth Systems*, *8*, 41–65. https://doi.org/10.1002/2015MS000526

Ranjram, M., & Craig, J. (2022). Upscaling hillslope-scale subsurface flow to inform catchment-scale recession behavior. *Water Resources Research*, *58*, e2021WR031913. https://doi.org/10.1029/2021WR031913

Rempe, D. M., & Dietrich, W. E. (2018). Direct observations of rock moisture, a hidden component of the hydrologic cycle. *Proceedings of the National Academy of Sciences of the United States of America*, *115*(11), 2664–2669. https://doi.org/10.1073/pnas.1800141115

Roques, C., Rupp, D. E., De Dreuzy, J.-R., Longuevergne, L., Jachens, E. R., Grant, G., et al. (2022). Recession discharge from compartmentalized bedrock hillslopes. *Hydrology and Earth System Sciences*, *26*(16), 4391–4405. https://doi.org/10.5194/hess-26-4391-2022

Sivapalan, M. (2018). From engineering hydrology to Earth system science: Milestones in the transformation of hydrologic science. *Hydrology and Earth System Sciences*, *22*(3), 1665–1693. https://doi.org/10.5194/hess-22-1665-2018

Tague, C., & Grant, G. E. (2004). A geological framework for interpreting the low-flow regimes of Cascade streams, Willamette River Basin, Oregon. *Water Resources Research*, *40*, W04303. https://doi.org/10.1029/2003WR002629

Tashie, A., Pavelsky, T., & Emanuel, R. E. (2020). Spatial and temporal patterns in baseflow recession in the continental United States. *Water Resources Research*, *56*(3), e2019WR026425. https://doi.org/10.1029/2019WR026425

Teuling, A., Lehner, I., Kirchner, J. W., & Seneviratne, S. I. (2010). Catchments as simple dynamical systems: Experience from a Swiss prealpine catchment. *Water Resources Research*, *46*, W10502. https://doi.org/10.1029/2009WR008777

Thomas, B. F., Vogel, R. M., Kroll, C. N., & Famiglietti, J. S. (2013). Estimation of the base flow recession constant under human interference. *Water Resources Research*, *49*, 7366–7379. https://doi.org/10.1002/wrcr.20532

Troch, P. A., Berne, A., Bogaart, P., Harman, C., Hilberts, A. G., Lyon, S. W., et al. (2013). The importance of hydraulic groundwater theory in catchment hydrology: The legacy of Wilfried Brutsaert and Jean-Yves Parlange. *Water Resources Research*, *49*, 5099–5116. https://doi.org/10.1002/wrcr.20407

Van Meter, K., Van Cappellen, P., & Basu, N. (2018). Legacy nitrogen may prevent achievement of water quality goals in the Gulf of Mexico. *Science*, *360*(6387), 427–430. https://doi.org/10.1126/science.aar4462

Wilusz, D. C., Harman, C. J., & Ball, W. P. (2017). Sensitivity of catchment transit times to rainfall variability under present and future climates. *Water Resources Research*, *53*, 10231–10256. https://doi.org/10.1002/2017WR020894

Wittenberg, H. (1999). Baseflow recession and recharge as nonlinear storage processes. *Hydrological Processes*, *13*(5), 715–726. https://doi.org/10.1002/(SICI)1099-1085(19990415)13:5<715::AID-HYP775>3.0.CO;2-N

Wlostowski, A. N., Molotch, N., Anderson, S. P., Brantley, S. L., Chorover, J., Dralle, D., et al. (2021). Signatures of hydrologic function across the Critical Zone Observatory network. *Water Resources Research*, *57*, e2019WR026635. https://doi.org/10.1029/2019WR026635

Wu, S., Zhao, J., Wang, H., & Sivapalan, M. (2021). Regional patterns and physical controls of streamflow generation across the Conterminous United States. *Water Resources Research*, *57*, e2020WR028086. https://doi.org/10.1029/2020WR028086

Yamazaki, D., Ikeshima, D., Sosa, J., Bates, P. D., Allen, G. H., & Pavelsky, T. M. (2019). MERIT hydro: A high-resolution global hydrography map based on latest topography dataset. *Water Resources Research*, *55*, 5053–5073. https://doi.org/10.1029/2019WR024873

References From the Supporting Information

Roques, C., Rupp, D. E., & Selker, J. S. (2017). Improved streamflow recession parameter estimation with attention to calculation of $-dQ/dt$. *Advances in Water Resources*, *108*, 29–43. https://doi.org/10.1016/j.advwatres.2017.07.013